(12) INTERNATIONAL APPLICATION PUBLISHED UNDER THE PATENT COOPERATION TREATY (PCT)

(19) World Intellectual Property Organization
International Bureau

(43) International Publication Date
02 February 2023 (02.02.2023)

WIPO | PCT

(10) International Publication Number
WO 2023/007496 A1

(51) International Patent Classification:
G01N 23/02 (2006.01) *G01T 1/29* (2006.01)
G01N 23/203 (2006.01)

(21) International Application Number:
PCT/IL2022/050814

(22) International Filing Date:
27 July 2022 (27.07.2022)

(25) Filing Language: English

(26) Publication Language: English

(30) Priority Data:
63/226,195 28 July 2021 (28.07.2021) US

(71) Applicant: **BAR ILAN UNIVERSITY** [IL/IL]; Bar Ilan University, 5290002 Ramat Gan (IL).

(72) Inventors: **COHEN, Eliahu**; 27B Har Hatzofim, 7662041 Rehovot (IL). **SHWARTZ, Sharon**; 9/7 Igal Alon St., 5503005 Kiryat Ono (IL). **BEN-YEHUDA, Adi**; 49 Palmach St., 3455848 Haifa (IL). **SEFI, Or**; 60 Menachem Begin, 4973260 Petach-Tikva (IL). **KLEIN, Yishay**; 21 Rural delivery south Lacish, 7936500 Amatzia (IL). **SUKHOLUSKI, Shimon**; Rehavat Rotem 10, 8251558 Kiryat Gat (IL).

(74) Agent: **STADLER, Svetlana**; COHN, DE VRIES, STADLER & CO., P.O.B 10278, 6110103 Tel Aviv (IL).

(81) Designated States *(unless otherwise indicated, for every kind of national protection available)*: AE, AG, AL, AM, AO, AT, AU, AZ, BA, BB, BG, BH, BN, BR, BW, BY, BZ, CA, CH, CL, CN, CO, CR, CU, CV, CZ, DE, DJ, DK, DM, DO, DZ, EC, EE, EG, ES, FI, GB, GD, GE, GH, GM, GT, HN, HR, HU, ID, IL, IN, IQ, IR, IS, IT, JM, JO, JP, KE, KG, KH, KN, KP, KR, KW, KZ, LA, LC, LK, LR, LS, LU, LY, MA, MD, ME, MG, MK, MN, MW, MX, MY, MZ, NA, NG, NI, NO, NZ, OM, PA, PE, PG, PH, PL, PT, QA, RO, RS, RU, RW, SA, SC, SD, SE, SG, SK, SL, ST, SV, SY, TH,

WO 2023/007496 A1

(54) Title: METHOD AND SYSTEM FOR HIGH PHOTON ENERGIES IMAGING

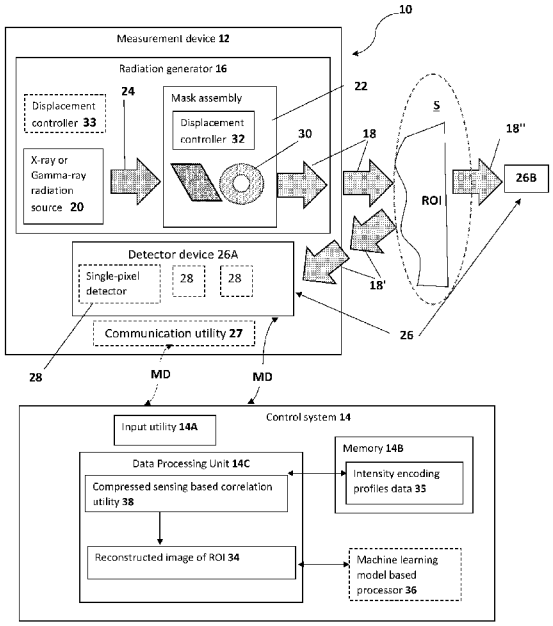


Fig. 1

(57) Abstract: A masking assembly is presented for use in inspecting a region of interest by creating structured high photon energy radiation to interact with the region of interest. The masking assembly comprises at least one mask structure, the mask structure having a predetermined effective thickness t, and comprising a mask pattern formed by an arrangement of spaced-apart features of absorption properties with respect to said high photon energy radiation different from spaces between said features. The arrangement of said features along a lateral dimension of the pattern defines a predetermined effective pattern size *P*. The features have a characteristic lateral size *I* providing a substantially high aspect ratio *t/l*.

[Continued on next page]

TJ, TM, TN, TR, TT, TZ, UA, UG, US, UZ, VC, VN, WS, ZA, ZM, ZW.

(84) **Designated States** *(unless otherwise indicated, for every kind of regional protection available)*: ARIPO (BW, GH, GM, KE, LR, LS, MW, MZ, NA, RW, SD, SL, ST, SZ, TZ, UG, ZM, ZW), Eurasian (AM, AZ, BY, KG, KZ, RU, TJ, TM), European (AL, AT, BE, BG, CH, CY, CZ, DE, DK, EE, ES, FI, FR, GB, GR, HR, HU, IE, IS, IT, LT, LU, LV, MC, MK, MT, NL, NO, PL, PT, RO, RS, SE, SI, SK, SM, TR), OAPI (BF, BJ, CF, CG, CI, CM, GA, GN, GQ, GW, KM, ML, MR, NE, SN, TD, TG).

Declarations under Rule 4.17:

— *of inventorship (Rule 4.17(iv))*

Published:

— *with international search report (Art. 21(3))*

METHOD AND SYSTEM FOR HIGH PHOTON ENERGIES IMAGING

TECHNOLOGICAL FIELD

The present invention is in the field of high photon energies imaging techniques and relates to X-ray or gamma-ray imaging system and method utilizing structured radiation for inspecting samples.

BACKGROUND ART

References considered to be relevant as background to the presently disclosed subject matter are listed below:

1. A. Geva, Y. Y. Schechner, Y. Chernyak, R. Gupta, Proc. European Conf. Computer Vision (ECCV 2018).

2. T. J. Lane and D. Ratner, Opt. Express 28, 5898 (2020).

3. M. J. Padgett and R. W. Boyd, Philos. Trans. R. Soc. A 375, 20160233 (2017).

4. A. -X. Zhang, Y. -H. He, L. -A. Wu, L. -M. Chen, and B. -B Wang, Optica 5, 374 (2018).

5. D. Pelliccia, A. Rack, M. Scheel, V. Cantelli, and D. M. Paganin, Phys. Rev. Lett. 117, 113902 (2016).

6. H. Yu et al., Phys. Rev. Lett. 117, 113901 (2016).

7. A. Schori, and S. Shwartz, Opt. Express 25, 14822 (2017).

8. A. M. Kingston et al., Optica 5, 1516 (2018).

9. A. Schori, D. Borodin, K. Tamasaku, and S. Shwartz, Phys. Rev. A 97, 063804 (2018).

10. Y. Klein, A. Schori, I. P. Dolbnya, K. Sawhney, S. Shwartz, Opt. Exp. 27, 3284 (2019).

10. N. D. Hardy and J. H. Shapiro, Phys. Rev. A 84, 063824 (2011).

11. F. Wang, H. Wang, H. Wang, G. Li, and G. Situ, Opt. Express 27, 25560 (2019).

Acknowledgement of the above references herein is not to be inferred as meaning that these are in any way relevant to the patentability of the presently disclosed subject matter.

BACKGROUND

X-ray and gamma-ray imaging methods are used for numerous applications in a variety of areas ranging from basic science to medicine, industry, and security. The main advantage of this very high photon energy radiation for imaging is its unique capability to penetrate through surfaces, which are opaque to other commonly used wavelengths, such as visible and infrared. However, despite the existence of many instruments and devices, which are based on X-ray and gamma-ray imaging, there are several physical limitations that restrict the resolution and contrast of these techniques.

The main fundamental challenge is the absence of high-quality lenses, thus high photon energy microscopes that operate like microscopes at optical wavelengths are devices that are very challenging to implement. There is a very fundamental physical reason for this challenge: the refractive index of any material in the high-photon energy range is nearly unity, thus the refractive index contrast between the lens material and the environment is tiny, leading to a very small magnification, which is impractical for imaging applications. From similar considerations, mirrors require very small grazing angles, which again are impractical. Moreover, the requirement for lens and mirror surfaces with roughness better than the wavelength is not possible since the wavelength is shorter than the size of one atom, thus phase distortions are induced. Lenses with very limited capabilities, which are also insufficient for practical applications, have been presented at photon energies up to about 150 keV but not at higher photon energies. In the absence of lenses, the spatial information for measurements at very high-photon energies is retrieved by using pixelated detectors and by measuring the intensity variation from one pixel to another. It is clear that with these detectors the resolution is limited by the pixel size. However, absorption is also weak in this photon energy range, which implies that the efficiency of the direct detection is small. To overcome this challenge, scintillation detectors are used. In those detectors, the photons are converted by a scintillation screen to visible photons, which are then detected by a visible-radiation-sensitive detector.

Nevertheless, even with scintillators, the efficiency depends on the absorption of the scintillation screen, thus the requirement for sufficient detection efficiency leads to firm requirements on the minimal thickness of the screen. Since the blurring introduced by the scintillation screen increases with the screen thickness, the resolution of the image is limited by the screen thickness. This fundamental challenge becomes more severe at higher photon energies as the absorption coefficient decreases.

Another challenge is also inherently related to the physics of X-ray and gamma-rays, namely, these are ionizing forms of radiation, threatening both the operators (e.g. technicians, surgeons) and subjects (e.g. patients, radiation-sensitive materials). Therefore, an important aim is to reduce the absorbed radiation power. Practical challenges include the current cost and size of X-ray and gamma-ray imaging devices.

GENERAL DESCRIPTION

There is a need in the art for a novel approach for inspecting samples by imaging using structured X-ray or gamma-ray radiation.

Traditionally, there are two approaches for active imaging: full field imaging where the whole object is measured by a two-dimensional (2D) detector and a scanning method in which a focused beam is used, and the sample is raster scanned. Another technique utilizes structured illumination, which enables to introduce spatial variations of intensity or phase, usually by a spatial light modulator (in the visible regime) or diffuser (in higher photon energies), and the image is acquired by measuring various realizations of the intensity or phase structures. This method has several potential advantages over the traditional methods. First, in structured illumination the resolution is limited by the variation of the intensity, which is introduced by the diffuser and not by the pixel size of the detector, thus higher resolution than that of standard 2D detectors can be achieved. For wavelength ranges such as X-rays and gamma-rays the insertion of a diffuser into the beam's path is vital due to the absence of high-quality, non-expensive lenses which could be used for full-field imaging or high-quality, computer controlled spatial light modulators which could be used for ghost imaging. Furthermore, since most objects/samples are either sparse or can be transformed into a basis where they are sparse, the number of required realizations can be made significantly lower than the data points with raster scanning. When combined with intensity correlation measurements, the flux of radiation on the object can be substantially reduced.

Ghost Imaging (GI) is an imaging scheme, which utilizes either classically or quantumly correlated radiation. This technique has received considerable attention throughout the years mainly with regards to visible radiation. The key idea of GI is to use two beams with identical intensity fluctuations. One of the beams is measured by a two-dimensional detector, but that beam does not interact with the object. The second beam interacts with the object and then it is collected by a single-pixel detector that has no spatial resolution.

The image is reconstructed by correlating the two measured intensities at the two detectors for many different realizations of input intensity fluctuation. Alternatively, and more practically, it is possible to perform two series of measurements; in the first step the diffuser is scanned without the object and the intensity distribution is recorded by using a high-resolution imaging system that included a pixelated detector or a pencil beam. In the second step the object is inserted, and the pixelated detector is replaced by a single-pixel detector. The diffuser is scanned again for the same realization as in the first step. Finally, the two series of data are correlated for the reconstruction of the image. This method is often called computational ghost imaging.

In recent years, several groups have demonstrated the possibility to utilize GI techniques for X-ray imaging and suggested that it can be used for dose reduction. GI was traditionally performed on transmissive objects, but it was shown that it can be applied also to reflective scenarios where the single-pixel detector is positioned next to the illumination source as in remote sensing applications. It was also shown that reflective GI through turbulent media can be properly addressed.

For at least the challenges described above, there remains a need for a radically new method that can surmount them and lead to new capabilities for high-photon energy measurements in general and for imaging in particular.

The technique of the present invention encompasses methods and systems for high photon energies imaging and their use for dose reduction in medical imaging and non-destructive imaging, for resolution improvement, and for reducing scattering effects or for a single-sided operation in X-ray and gamma-ray measurements. The present invention utilizes detection of elastic and inelastic (Compton) scattering. In this connection, it should be noted that although such Compton scattering often reduces the contrast of the reconstructed image and leads to image blurring and reduction in the sensitivity of the measurements, the technique of the present invention utilizes a

specifically designed structured radiation enabling to significantly improve the image resolution extracted from detection of Compton scattering.

Typically, the X-ray or gamma-ray source may be X-ray tube, radioactive nuclei, positron-electron annihilation, or inverse Compton scattering source. In the description below, the radiation source and emitted radiation are referred to as "X-ray source" and "X-ray radiation".

The present invention provides a novel design of a mask assembly and its operation to sequentially produce mutually different spatially encoded X-ray beams interacting with a region of interest being inspected. The mask structure (which may for example be configured as a plate-like structure) has a predetermined effective thickness t, and is formed with a pattern of an arrangement of spaced-apart features of different absorption of the high photon energy radiation used in the inspection as compared to that of spaces between them. The pattern has a predetermined pattern size defined by the arrangement of these features along a lateral dimension of the pattern. The features have a characteristic lateral size l providing a substantially high aspect ratio t/l.

Typically, the mask pattern may be in the form of a 3D printed structured and/or spongy or porous materials; or the mask may comprise structures created by laser ablation. In some embodiments, the mask pattern is optimized using advanced algorithms such as compressed sensing or deep learning algorithms.

The technique of the invention provides high-resolution, high-contrast low-dose imaging at hard X-rays and/or gamma-rays, which may be further optimized by tailoring the mask pattern to a particular class of objects (regions of interest) or a specific object within a certain class, designing the compressed sensing algorithm and reconstruction algorithm in accordance with both mask pattern and object.

Detector(s) used to collect/detect radiation responses of the region of interest to the differently encoded X-ray beams include single-pixel detector or an array of single-pixel detectors or a flat panel.

The method for high-resolution, high-contrast low-dose imaging at hard X-rays and/or gamma-rays may further comprise digital image processing algorithms (e.g. denoising or edge enhancement), as well as automatic target recognition, classification and diagnosis.

The present disclosure also comprises a method for designing the masks/diffusers of the present disclosure. The method comprises planning the mask with both sufficient

randomness and spatial thickness variance. Here, an algorithm, which provides the optimal results (that is best image quality with lowest required dose) is used; then the sparsity nature of the objects, for example, for various organs in the human body, is used to determine the reduction of the dose and the number of realizations, by using GI simulations combined with compressed sensing and/or machine learning (ML) tools. The structure of the mask/diffuser of the present disclosure may be further optimized by obtaining the cost function, which is the number of required realizations for obtaining the object's image with the best SNR. In order to obtain the cost function, ML tools, such as Support Vector Machine and deep learning using Artificial Neural Networks, may be used.

It should be noted that the present invention provides automatic classification of the regions of interest based on the results of the inspection (reconstructed image of the region of interest). The invention can advantageously be used in computed tomography, and in particular medical imaging, fluoroscopy, microscopy, non-destructive measurements.

According to one broad aspect of the invention, there is provided a masking assembly for use in inspecting a region of interest by creating structured high photon energy radiation to interact with the region of interest. The masking assembly comprises: at least one mask structure, the mask structure having a predetermined effective thickness t, and comprising a mask pattern formed by an arrangement of spaced-apart features of absorption properties with respect to said high photon energy radiation different from spaces between said features, said arrangement of said features along a lateral dimension of the pattern defining a predetermined effective pattern size P, wherein the features have a characteristic lateral size l providing a substantially high aspect ratio t/l.

In some embodiments, the mask structure has a spatial modulation of thickness along the pattern within said effective thickness t.

The mask structure may be a disk-like structure, where the spaced-apart features of the mask pattern are arranged along a substantially circular path.

The mask assembly may further include a drive mechanism configured and controllably operable as a displacement controller to implement successive lateral movements of said mask pattern with a predetermined lateral jump j to thereby enable successive inspection realizations through different segments of the mask pattern,

respectively, wherein a value of said lateral jump $j \neq N \times P$, N being an integer. For example, the predetermined lateral jump j is smaller than P.

The aspect ratio t/l is at least 10, and preferably 10 or higher.

In some embodiments, the mask pattern is formed by relatively highly absorbing features arranged in the spaced-apart relationship in a relatively low-absorbing substrate with respect to said high photon energy radiation. In some other embodiments, the mask pattern is formed by relatively low-absorbing features arranged in the spaced-apart relationship in a relatively highly absorbing substrate with respect to said high photon energy radiation. The relatively high absorbing material of the mask pattern may include metal material composition or polymer-based material compositions.

Considering the metal material composition, this may include one or more of the following: tungsten, platinum, silver, gold and tantalum.

The mask pattern may be produced by metal printing of the spaced-apart features, followed by laser milling.

In some embodiments, the mask pattern is in the form of distribution of pores in the relatively highly absorbing substrate. Such substrate may for example be made from one or more of the following: Limestone, Mortar, AlCu, MgZn.

In some embodiments, the mask pattern comprises an arrangement of the features providing desired sparsity in a predetermined base selected in accordance with base of sparsity in the region of interest being inspected. For example, the arrangement of said spaced-apart features of the mask pattern is selected in accordance with a certain function, e.g., function corresponding to discrete cosine transform or the like, e.g. wavelet.

In some other embodiments, the mask pattern comprises a random arrangement of said spaced-apart features.

According to another broad aspect of the invention, it provides an inspection system for inspecting a region of interest, the inspection system comprising: a measurement device configured and operable to perform a plurality of successive measurements of the region of interest by implementing a corresponding plurality of interactions of the region of interest with high photon energy radiation beams having predetermined different spatially encoded intensity profiles, and a detection system comprising at least one radiation detector device successively collecting radiation responses of the region of interest to said interactions and generating measured data indicative thereof, wherein said high photon energy radiation beams having

predetermined different spatially encoded intensity profiles are sequentially produced by passing an initial high photon energy radiation beam through the above-described masking assembly.

The at least one radiation detector device is configured and operable to collect said response of the region of interest comprising Compton scattering of the region of interest. The at least one radiation detector device may be accommodated for collecting at least one of back propagating and forward propagating radiation of said Compton scattering of the region of interest.

The inspection system also includes or is connectable to a control system configured and operable to process the measured data, thereby enabling reconstruction of image of the region of interest from said measured data by applying thereto at least one of compressed sensing based correlation processing and/or machine learning based processing, and generate data indicative of reconstructed image of the region of interest.

According to yet further broad aspect of the invention, it provides an inspection system for inspecting a region of interest, the inspection system comprising:

a measurement device configured and operable to perform a plurality of successive measurements of the region of interest by implementing a corresponding plurality of interactions of the region of interest with high photon energy radiation beams of X- or gamma-radiation having predetermined different spatially encoded intensity profiles, and a detection system comprising at least one radiation detector device configured and operable to successively collect radiation responses of the region of interest to said interactions and generate measured data indicative thereof, wherein said at least one radiation detector device is configured and operable to collect said response of the region of interest comprising Compton scattering of the region of interest including at least one of back propagating and forward propagating radiation of said Compton scattering of the region of interest, thereby enabling reconstruction of image of the region of interest from said measured data by applying thereto at least one of compressed sensing based correlation processing and machine learning based processing.

The inspection system may include a communication utility for communicating said measured data to a control system configured to perform said at least one of the compressed sensing based correlation processing and the machine learning based processing of the measure data and generate the reconstructed image of the region of interest. Alternatively or additionally, the inspection system includes a control system

configured to perform said at least one of the compressed sensing based correlation processing and the machine learning based processing.

The measurement device comprises: a source of the X-ray or gamma-ray radiation configured to provide an input beam of said radiation; and a mask assembly accommodated in a general propagation path of said input beam, the mask assembly comprising at least one mask structure being configured and controllably operated to sequentially induce different intensity fluctuations on the input beam, thereby sequentially producing beams of the X- or gamma-radiation having predetermined different spatially encoded intensity profiles. The mask structure has a predetermined effective thickness t, and comprises a mask pattern formed by an arrangement of spaced-apart features of absorption properties with respect to said high photon energy radiation different from spaces between them, said arrangement of said features along a lateral dimension of the mask pattern defining a predetermined effective pattern size P, wherein the features have a characteristic lateral size l providing a substantially high aspect ratio t/l.

The inspection system further includes a drive mechanism configured and controllably operable to implement successive lateral displacements between the general propagation path of the input beam and said mask pattern with a predetermined lateral jump j to thereby enable successive inspection realizations through different segments of the mask pattern, respectively, wherein a value of said lateral jump $j \neq N \times P$, N being an integer.

The invention also provides a method for inspecting a region of interest by X-rays or gamma rays radiation comprising:

i) producing an input beam of X-ray or gamma-ray radiation directed along a general propagation path towards the region of interest;

ii) scanning, by the input beam on its way towards the region of inters, a mask pattern, thereby sequentially inducing different intensity fluctuations in the input beam and producing a sequence of beams of the X- or gamma-radiation having predetermined different spatially encoded intensity profiles propagating towards the region of interest to successively interact with the region of interest and induce radiation a corresponding sequence of radiation responses of the region of interest comprising Compton scattering of the region of interest, said scanning being implemented by successive lateral displacements between the general propagation path of the input beam and said mask

pattern with a predetermined lateral jump j of a value satisfying a condition $j \neq NxP$, where N is an integer and P is a predetermined effective pattern size P of the mask pattern;

iii) detecting said sequence of the radiation responses comprising at least one of back propagating and forward propagating radiation of said Compton scattering of the region of interest and generating measured data indicative thereof, thereby enabling reconstruction of image of the region of interest from said measured data by applying thereto at least one of the compressed sensing based correlation processing and the machine learning based processing.

BRIEF DESCRIPTION OF THE DRAWINGS

In order to better understand the subject matter that is disclosed herein and to exemplify how it may be carried out in practice, embodiments will now be described, by way of non-limiting examples only, with reference to the accompanying drawings, in which:

Fig. 1 illustrates, by way of a block diagram, the inspection system according to the principles of the present invention;

Fig. 2 illustrates schematically the principles of configuring the mask pattern according to the present invention;

Fig. 3A illustrates an example of two step GI-based inspection technique of the invention;

Fig. 3B shows a specific example of a computer-designed mask suitable for use in the present invention; and **Fig. 3C** shows a photo of said mask;

Fig. 3D exemplifies a specific configuration of the system of the invention utilizing the two single-pixel detectors collecting backward scattered radiation response of a region of interest to spatially encoded radiation;

Fig. 4 shows the mask used for simulations and its various realizations;

Figs. 5A to 5F show the process and results of simulations where the original image (Fig. 5A) was reconstructed with various auto-correlation lengths (ACL) and jumps;

Fig. 6 shows schematically machine learning based image reconstruction suitable to be used in the invention;

Figs. 7A to 7C show simulations of resolution improvement for chest X-ray, wherein **Fig. 7A** shows a high-resolution image taken from images' bank; **Fig. 7B** shows the same image as **Fig. 7A** with artificially downgraded resolution; and **Fig. 7C** shows the simulated image using GI-based reconstruction scheme;

Figs. 8A to 8B show simulations of compression for orthopedic images, wherein **Fig. 8A** shows a high-resolution image taken from images' bank; and **Fig. 8B** shows the result of GI simulation using compression ratio of 30 and a discrete cosine transform (DCT) basis for reconstruction; and

Figs. 9A to **9B** illustrate imaging of the Hebrew letter 'Aleph' (א), wherein **Fig. 9**A shows experimental results of direct imaging; and **Fig. 9B** shows results of imaging using GI with about 500 realizations for the reconstruction of the 5000-pixel image.

DETAILED DESCRIPTION OF EMBODIMENTS

The present disclosure encompasses systems and methods for high photon energies imaging. The present disclosure further comprises use of the systems and methods of the present disclosure for dose reduction in medical and non-destructive imaging, for resolution improvement, and for reducing scattering effects or for a single side operation in X-ray and gamma-ray measurements.

The present disclosure addresses the challenges associated with X-ray and gamma-ray imaging described above by utilizing a new approach that relies on: (1) Manipulating the structure of the beam that interacts with the object while employing advanced computational models; (2) Using correlation measurements; and (3) Combining the first two approaches with ML approaches.

Reference is made to **Fig. 1** illustrating, by way of a block diagram, an inspection system **10** configured and operable according to the principles of the present invention for inspecting a region of interest in a sample **S** (subject / object) and determining data indicative of a spatial structure of the region of interest, e.g. carrying information about defects / abnormalities of the region of interest. The system **10** is configured and operable to implement general principles of X- or gamma-ray based GI utilizing a sequence of interactions between the region of interest with different structured radiations, respectively.

The system of the invention can be used in various applications, including medical and other applications, such as computed tomography, fluoroscopy, microscopy, as well as non-destructive measurements. The latter can be used in inspection of samples for defects and other abnormalities.

The system **10** includes a measurement device **12** and is associated with a control system **14**, i.e., includes or is connectable with the control system. As shown in the figure, the measurement device may include a communication utility **27** having any known suitable configuration for wireless data communication with the control system.

The measurement device **12** is configured and operable to perform a plurality of successive measurements of the region of interest by implementing a corresponding plurality of interactions of the region of interest with X-ray or gamma-ray radiation beams having predetermined different spatially encoded intensity profiles**.** In the description below, such radiation is referred to as X-ray radiation.

The measurement device **12** includes a radiation generator **16** configured and operable to sequentially produce such beams of X-ray or gamma-ray radiation having predetermined different spatially encoded intensity profiles **18** propagating towards a region of interest **ROI**; and a detection system **26** including at least one detector device **26A** and/or **26B** (each including one or more detectors **28** being preferably single-pixel detector(s)) configured and operable to collect successively induced responses of the region of interest to the interactions with said X-ray or gamma-ray radiation beams having predetermined different spatially encoded intensity profiles and generate measured data **MD** indicative thereof. The response of the region of interest being detected includes Compton scattering of the region of interest. The detection system **26** may include the detector device **26A** accommodated to detect radiation response **18'** corresponding to back scattering of the spatially encoded radiation **18** from the region of interest and/or to detect radiation response corresponding to transmission **18''** of said radiation **18** through the region of interest.

The inventors have shown that collecting radiation **18'** back scattered from the sample might be sufficient to obtain all required information about the spatial structure of the sample, while enabling the inspection system of simpler configuration, smaller in footprint and weight. Also, the inventors have shown that the inspection results may be further optimized by detecting the back scattered radiation **18'** propagating along a path

with as small as possible angular orientation with respect to the general propagation path of radiation **18**.

The detector **28** may be a single pixel detector. The detector can use angular and/or spectral information. It should be understood that with the use of measured data including a sequence of measured data pieces indicative of a corresponding sequence of the radiation responses embedding different spatially encoded M intensity patterns, image of the region of interest can be reconstructed from the measured data with certain spatial resolution $p \times q$ (as if there were a matrix of $p \times q$ pixels), where $p \times q = N, N \gg M$. To this end, compressed sensing based image processing is typically used, utilizing correlation between the M measured data pieces and prior knowledge of respective image data about the M mask pattern segments used in the respective realizations.

The present invention provides ways for implementing such technique with a reduced number M of realizations/acquisitions, and thus lower dose of radiation applied to the region of interest, and potentially shorter inspection session, as well as simpler, smaller and lighter mask. This is achieved by an optimized configuration of the mask structure and its displacement to provide the sequence of beam interactions with different mask pattern segments. This will be described more specifically further below.

The radiation generator **16** includes a radiation source **20** producing a beam of X-ray or gamma-ray radiation **24** (of a predetermined spectral range). The radiation generator further includes a mask assembly/unit **22** which includes at least one mask defining a mask pattern formed by an arrangement of spaced-apart features of absorption properties with respect to said radiation different than that of spaces between these features.

The radiation generator **16** is configured to provide controllable relative displacement between the mask pattern and a general propagation path of the input radiation beam **24** such that the beam **24** sequentially passes through different (mutually different) segments of the mask pattern thus resulting in a sequence if differently spatially encoded beams sequentially interacting with the region of interest.

As shown in the figure, in some embodiments, the mask is controllably laterally displaceable/movable with respect to the general propagation path of the radiation beam **24** to cause said beam to successively pass through different pattern segments of the mask pattern to thereby induce different spatial encoding in the intensity profile of the beam. To this end, the mask assembly includes a drive mechanism / displacement controller **32**

configured and operable to control displacement (e.g., rotation of a disk-like pattern) with respect to the propagation path during an inspection session to implement a plurality of M different realization / acquisitions with M mutually different spatially encoded radiation distributions **18**.

Alternatively, or additionally, to the mask pattern displacement with respect to the input beam propagation path, the input beam **24** propagation path can be controllably displaced with respect to the mask pattern using a respective displacement controller **33**.

The displacement of the mask pattern with respect to the radiation propagation path is implemented with a predetermined lateral step / jump j the value of which is selected such that it is different from $k \times P$, where k is an integer and P is a predetermined effective pattern size P of the mask pattern. The preferred embodiments for the mask pattern configuration are described further below.

The control system **14** is generally a computer system including *inter alia* such functional utilities as input utility **14A**, memory **14B** and data processor **14C**. As indicated above, the control system **14** may be part of the measurement device **12** or may be a remote system in data communication with the measurement device (with the detection system) via a communication network. It should be noted that data processing modules may be distributed between a local controller of the measurement device and the remote control system, as the case may be.

The control system **14** is configured and operable to process the measured data **MD** to obtain reconstructed image of the region of interest **34**. This can be implemented using a compressed sensing based correlation utility **38** configured and operable based on the general principles of compressed sensing based image processing utilizing correlation between the M measured data pieces and prior knowledge of respective image data about the M mask pattern segments, i.e. intensity encoding profiles data **35** stored in the memory **14B**, used in the respective realizations. Alternatively, utilizing machine learning model based data processor **36** can be used.

The mask pattern includes an arrangement of spaced-apart features which differ from the spaces between them in the interaction properties with said radiation **24**, e.g., absorption, transmission, scattering of said radiation. The mask pattern operates as a radiation diffuser and may be transversely / laterally displaceable with respect to the radiation propagation path (e.g. via rotation in a plane substantially perpendicular to the radiation propagation path) using a predetermined lateral displacement step / jump.

The pattern may include a periodic (or almost periodic) arrangement of features, or arrangement according to a certain known function. In some embodiments, the mask includes a random arrangement of features. Thus, passage of radiation **16** through the patterned segment of the mask results in the spatially encoded radiation **18** which interacts with the region of interest.

Reference is made to **Fig. 2** schematically illustrating the main principles for configuring the mask structure **30** and the mask pattern. It should be understood that the figure is schematic, not in scale, and the pattern is simplified just in order to simplify the description of the main features thereof.

The mask structure **30** (e.g. plate-like structure) has a certain predetermined effective thickness ***t*** and is formed with a predetermined pattern of the arrangement of spaced-apart features **F** which have different absorption properties (and thus transmission) with respect to the X-ray radiation used in the inspection procedure as compared to that of spaces between them. In some embodiments, the mask structure (e.g. plate-like structure) is configured with spatial modulation of thickness along the pattern within said effective thickness *t*.

For example, the features **F** are relatively highly absorbing (less transmissive) than the spaces between these features, or alternatively, features **F** are almost non-absorbing in highly-absorbing bulk of the mask structure. It should also be noted that the pattern may be such that the features **F** as well as spaces between them, although being relatively transmissive and absorbing, the features **F** may be different between them in the respective property, and similarly, the spaces nay be different between them in their respective properties.

Thus, generally speaking, the mask pattern is in the form of varying transmission with respect to said X-ray radiation, where either highly absorbing features are arranged in the spaced-apart relationship in a relatively low-absorbing substrate with respect to said high photon energy radiation, or relatively low-absorbing features are arranged in the spaced-apart relationship in a relatively highly absorbing substrate. The relatively high absorbing material of the mask pattern may include metal material composition(s), e.g. one or more of the following: tungsten, platinum, silver, gold and tantalum.

The mask pattern may be produced by metal printing of the spaced-apart features, followed by laser milling, in the low-absorbing substrate of the mask structure.

Alternatively, the mask pattern may be in the form of distribution of pores in the relatively highly absorbing substrate.

For example, the arrangement of features may be random or quasi-random. In some embodiments, the mask structure (plate-like structure) is configured with both the spatial modulation of thickness and the randomness of the pattern.

The feature **F** has a characteristic lateral size l, such that a substantially high aspect ratio t/l is achieved (e.g., the aspect ratio of at least 10). The pattern (arrangement of features **F**) has its predetermined effective pattern size **P**. Such pattern size **P** presents a so-called "correlation length" of the mask, which describes an "effective pixel size", corresponding to the number of adjacent pixels of the same value in the assumed pixel matrix $p \times q$ of the required spatial resolution of the reconstructed image. This is actually an autocorrelation characteristic of the mask pattern.

Further, according to the invention, the displacement controller **32** is configured and operable to provide optimized controllable lateral displacement jump ***j*** of the mask/pattern such that $j \neq k \times P$, k being an integer. More specifically, the jump ***j*** may be smaller or larger than ***P*** but should not be of the value of multiplication of ***P***.

In some embodiments, the mask pattern is such that the arrangement of features **F** provides desired sparsity in a predetermined base, which is selected in accordance with the base of sparsity in the region of interest. To this end, a preliminary imaging may be performed once for a given region of interest using the same X-ray radiation with no spatial encoding of such radiation (no mask) and using a pixelated detector, and analyze the image data to identify the base of sparsity of the region of interest.

With some prior knowledge regarding the type and size of the imaged object, this can be made even without the preliminary imaging stage.

In some other embodiments, the arrangement of features **F** in the mask pattern is selected in accordance with a certain function, e.g. a function corresponding to discrete cosine transform. This will be described further below.

The jump-by-jump lateral displacement of the mask pattern with respect to the general propagation path of X-ray radiation results in successive location of different pattern segments in the propagation path of the radiation thus differently encoding such radiation. The mask patterns (or pattern segments of the mask) may be a-priori known (predetermined, e.g. according to a certain function) and fabricated based on a computer-generated predesigned map. Alternatively, the patterns may be unknown and previously

(prior to inspection) characterized using a high-resolution system. To this end, the spatial intensity profiles of the X-ray radiation induced by the pattern segments can be previously studied by interacting the X-ray radiation with each pattern segment, detecting the response of the pattern segment (transmission or reflection) by a pixelated detector, and storing the respective image data. Such technique is generally known and used in GI applications.

Reference is made to **Fig. 3A** schematically exemplifying the configuration and operation of the inspection system **10** of the invention. In this example, the system **10** includes a standard X-ray source **20** typically used for medical imaging. As shown in the fire, the pattern segments of the mask **30** is first learned using an imaging system **100**, which utilizes the same X-ray source **20** and a pixelated detector **40**. It should be understood that the mask is laterally displaced (e.g. rotated) and the input beam **24** thus successively interacts with (passes through) a different pattern segment and is then detected by the pixelated detector **40**. It should be understood that the imaging plane (radiation sensitive surface of the pixelated detector) is the same or conjugate plane of the detector **26A** (or **26B**) which is then used in the inspection of the region of interest.

The mask **30** may be fabricated by either nanotechnology or 3D printing, where two materials (e.g. stainless steel and a polymer) may be used to achieve the high absorption contrast that introduces the structured illumination. According to said procedures, the patterns of the mask are predesigned, using a computer code, for example, by using MATLAB, and the fabrication of the mask is performed according to the design. For example, this may be a computer-generated mask. According to this procedure, the landscape of the mask is known and is used to calculate the intensity fluctuations at the object position.

In the experiments conducted by the inventors, the structure of the mask was predesigned with a MATLAB code, hence the structure of the fluctuation intensity was known in the entire range of realizations. **Figs. 3B and 3C** illustrate the designed mask and a photo of the mask. The mask **30** shown in **Fig. 3B** is designed to be used at 661 keV gamma-ray radiation. The average lateral feature size is about 110 μm and its height (mask plate thickness) is about 1.5 mm. Therefore, correlation length (effective pattern size) is also about 110 μm and the spatial resolution of the mask image is comparable.

During the inspection of the region of interest, the mask is preferably positioned as close as possible to the object (containing the region of interest) in order to avoid

magnification of the feature size of the mask in the image plane (defined by the single pixel detector). The mask pattern is scanned (i.e. via lateral displacement of the mask in one or two lateral dimensions), and the successive differently encoded responses of the region of interest are detected by the single-pixel detector **26A** (and/or **26B**) and the corresponding successive measured data pieces (forming the measured data) are recorded (stored). Then, this measured data is processed and the image of the region of interest is reconstructed. This may be done using any known suitable technique based on correlation of the radiation intensity measured by the single-pixel detector and the intensity profile of the mask pattern (pattern segment) for each of the realizations.

For lower photon energies of X-ray radiation, masks with smaller features are used, thereby improving the spatial resolution. This is possible since the absorption of materials is larger at lower photon energies and thus the intensity induced fluctuations by a thin mask are more significant in this range. Since the mechanical constraints limit the ratio between the thickness of the feature and its lateral dimensions, the low absorption at high photon energies leads to the requirement of millimeter scale thicknesses, and therefore the lateral dimensions are about 100 microns. However, at lower photon energies it is possible to use even thicknesses on the order of 10 microns. For example, in mammography the typical photon energy is between 20 keV and 30 keV. In this range masks with feature sizes down to 10 microns, which are made either from porous materials or that are made by photolithography, are used. For the porous materials, their pattern is to be measured before the measurement/inspection of the object, and the two-step approach described above with reference to Fig. 3A is used. The mask is therefore positioned to modulate the intensity of the input beam **24** in the absence of the object, and the patterns of the masks (pattern segments of the same mask) are imaged for the various realizations that are used in the second step where the object is measured/inspected. In the second step, the object (region of interest) to be inspected is located in the path of the X-ray radiation **24** and the intensity is measured by the single-pixel detector(s) as described above. As with the known mask, the computational approach described above is used to reconstruct the image of the object (region of interest).

For the intermediate energy range of 30 keV-100 keV, which is routinely used for various medical examinations, mask patterns with feature sizes of about 20-50 microns can be used, improving thereby the state-of-the-art medical imaging resolution. As described above, the constraint is the ratio between the thickness and lateral dimensions

of the features (aspect ratio t/l), which depends on the details of the manufacturing technique, and is at least 10, i.e. at least one order of magnitude higher, and preferably 3 or more orders of magnitude higher. There are many suitable known techniques for the fabrication of the mask, for example three-dimensional metal printing and laser milling of heavy elements (e.g., tungsten or platinum).

When using the Compton scattering, which is the dominant scattering mechanism in the X-ray regime, the procedure for the image reconstruction may be generally similar to the above-described compressed sensing and correlation based technique, but the detector is to be positioned to collect the Compton scattered signal (detector **26A**) instead of or in addition to the transmitted signal (detector **26B**). Since the single-pixel detector has no spatial resolution, it is not sensitive to the angle of the scattered radiation in contrast to standard pixelated detectors.

The inventors have shown that using the technique of the invention utilizing detection of the Compton effect scattering with the single-pixel detector(s) allows to reconstruct the image of the region of interest even when the source and the detector are on the same side of the object (i.e. backward propagating response of the region of interest).

The schematic of the experimental setup is depicted in **Fig 3D** in a self-explanatory manner where two such single-pixel detectors **26A** are used to collect backward propagating responses of the region of interest substantially symmetrically with respect to the general propagation path.

As indicated above, the mask pattern (arrangement features of different properties with respect to the X-ray radiation) can be designed in accordance with a predetermined function. The inventors have shown that the function corresponding to a discrete cosine transform (DCT) can be used in the above described configuration of the mask. The following is the theoretical explanation supported by simulations conducted by the inventors.

In ghost imaging a mask/diffuser (D) is used to illuminate an object ($\vec{x}$) and accumulate all the transmitted (or reflected/scattered) radiation into a bucket detector ($\vec{b}$) (e.g., a single-pixel detector) a number of times (M realizations). For each realization, the mask/diffuser D is moved so that each successive realization utilizes a different pattern segment and is different from the preceding one, and at each realization a virtual matrix

$p \times q$ of pixels of the respective pattern segment of the mask/diffuser is exposed to the process. By measuring the transmission (or reflection) of diffuser D, the object $\vec{x}$ (with resolution of $p \times q$ pixels) may be reconstructed via the bucket readings $\vec{b}$.

The following equation describes the measurement process using here, for simplicity, a one-dimensional problem (in the case of a two-dimensional object whose size is [p × q] pixels, the total number of pixels, N, is N = p × q):

$$Dx = b \qquad (1)$$

where D is an $M \times N$ matrix of the diffuser/mask pattern whose rows are the M different realizations (mask transmission/scattering realizations) for each pixel in the virtual matrix p × q, $\vec{x}$ is the N (unknown) object transmission/scattering values for each pixel and $\vec{b}$ is the vector of bucket detector measurements (e.g., single-pixel detector) for each mask realization. Mask realizations could be obtained using the same physical mask translated or rotated in front of the source. Each mask position corresponds to one measurement/realization.

Using compressed sensing, it is possible to obtain more information with fewer (i.e., smaller number M) of measurements by treating the process as a constraint of linear equations (size of $M \times p \times q$) and trying to minimize various possible norms.

In the following, the inventors show that with a certain diffuser / mask pattern, the norm of a gradient (as well as the norm of higher derivatives) is already minimal. Therefore, here lies a degree of freedom to choose a different norm to minimize or to satisfy other constraints.

In general, ghost imaging (GI) uses the following set of linear equations (respectively, for one-dimensional (1D) and two-dimensional (2D) problem):

$$\begin{cases} D\vec{x} = \vec{b} & 1D \\ \sum_{j,k} D_{ijk}\, x_{jk} = b_i & 2D \end{cases} \qquad (2)$$

The number of measurements is the number of rows in D (denoted by i), and hence, if there are enough measurements, then D is invertible. To try and minimize the number of measurements (and therefore the amount of radiation) the inventors employed various compressed sensing techniques.

In the Total Variation Algorithm 3 (TVAL3) one tries to minimize Eq. (3)

$$\mathcal{L} = \begin{cases} \alpha\left|D\vec{x} - \vec{b}\right|_2 + \beta|\nabla x|_1 & 1D \\ \alpha\left|D\vec{x} - \vec{b}\right|_2 + \beta\left(\left|\partial_x x\right|_1 + \left|\partial_y x\right|_1\right) & 2D \end{cases} \quad (3)$$

or, in an alternative notation:

$$\mathcal{L} = \begin{cases} \alpha\sqrt{\sum_i \left(\sum_j D_{ij}\, x_j - b_i\right)^2} + \beta \sum_j \left|x_{j+1} - x_j\right| & 1D \\ \alpha\sqrt{\sum_i \left(\sum_{j,k} D_{ijk}\, x_{jk} - b_i\right)^2} + \beta \sum_{j.k} \left(\left|x_{j+1,k} - x_{j,k}\right| + \left|x_{j,k+1} - x_{j,k}\right|\right) & 2D \end{cases} \quad (4)$$

If $\alpha \gg \beta$ (which usually is, otherwise one would obtain a flat line where the gradient is zero), then the corresponding constraint is more important. It can be seen that if the diffuser rows are orthogonal the object can be reconstructed using these vectors minimizing $|D\vec{x} - b|_2 = 0$ (or $|D\vec{x} - b|_2 \approx 0$ if $\alpha \not\gg \beta$) and to uphold that constraint one is allowed only to change the orthogonal complements (or very little of the diffuser vectors so that $|D\vec{x} - b|_2 \approx 0$).

The next step is to transform the diffuser matrix and the object vector to the basis in which the object is sparse. The transform which is used here for the analysis is the discrete cosine transform (DCT). However, this could be any other transform which satisfies the conditions of compressive sensing which are: (1) that the signal has a sparse representation in this basis; and (2) that the measurement basis is incoherent with the basis in which the signal is sparse.

The discrete cosine transform (DCT) algorithm is commonly used for image compression. It converts the pixels in an image into sets of spatial frequencies and is closely related to the DFT (Discrete Fourier Transform). Each realization is a basis vector of the discrete cosine transform (DCT), as will be explained in detail in the following. The discrete cosine transform (DCT) in 1D is defined as:

$$C[l] = \sqrt{\frac{2}{q}} \sum_{i=0}^{q-1} c\,[k] \cos\left(\frac{\pi}{q}\left(k + \frac{1}{2}\right) l\right) \quad (5)$$

where $c[k]$ is the k^{th} pixel of object c , and $C[l]$ is the l^{th} pixel of the DCT (counting from 0 to $q - 1$). To get the transformation matrix and how it looks in real space one needs to apply the inverse DCT (IDCT) to each row of the identity matrix. Each row of the identity is a basis vector. Thus, essentially, it amounts to just transforming the basis

vectors. Then each row in the transformation matrix will represent a DCT basis vector. The IDCT is:

$$c[k] = \sqrt{\frac{1}{q}}C[0] + \sqrt{\frac{2}{q}}\sum_{l=1}^{q-1} C\,[l]\cos\left(\frac{\pi}{q}\left(k+\frac{1}{2}\right)l\right) \qquad (6)$$

For the i^{th} vector the following is obtained:

$$c_i[k] = \sqrt{\frac{1}{q}}C_i[0] + \sqrt{\frac{2}{q}}\sum_{l=1}^{q-1} C_i\,[l]\cos\left(\frac{\pi}{q}\left(k+\frac{1}{2}\right)l\right) \qquad (7)$$

Because the identity matrix is transformed: $C_i[l] = \delta_{il}$

$$\begin{aligned} c_0[k] &= \sqrt{\frac{1}{q}}\delta_{i0} + \sqrt{\frac{2}{q}}\sum_{l=1}^{q-1}\delta_{l0}\cos\left(\frac{\pi}{q}\left(k+\frac{1}{2}\right)l\right) = \sqrt{\frac{1}{q}} \\ c_{i\neq 0}[k] &= \sqrt{\frac{1}{q}}\delta_{i0} + \sqrt{\frac{2}{q}}\sum_{l=1}^{q-1}\delta_{il}\cos\left(\frac{\pi}{q}\left(k+\frac{1}{2}\right)l\right) = \sqrt{\frac{2}{q}}\cos\left(\frac{\pi}{q}\left(k+\frac{1}{2}\right)i\right) \end{aligned} \qquad (8)$$

Since $\{C_i[l]\}_{i=0}^{q-1}$ are orthonormal and the transformation is unitary, it imposes that $\{c_i[k]\}_{i=0}^{q-1}$ are also orthonormal (Because the inner product doesn't change under the transformation). Meaning $\sum_{k=0}^{q-1} c_i\,[k]c_j[k] = \delta_{ij}$.

The inventors use $\{c_i[k]\}_{i=0}^{M}$ as the form for the DCT based diffuser with M realizations. The compact form can be introduced:

$$c_i[k] = a_i\cos(\omega_i k + \phi_i) \qquad (9)$$

where $a_i = \sqrt{\frac{2-\delta_{i0}}{q}}$ includes the normalization constant, $\omega_i = \frac{\pi i}{q}$ is the frequency, $\phi_i = \frac{\pi i}{2q}$ is the phase and k is the k^{th} pixel.

Following the previous logic, the next picture/image (i.e., required pixels of the object) in 1D (suggesting $p = 1$, but it can be naturally extended to 2D) is as follows:

$$x(k) = \sum_{i=0}^{q-1} c_i\,[k] = \sum_{i=0}^{q-1} a_i\cos(\omega_i k + \phi_i) \qquad (10)$$

Now, taking a gradient with respect to k one obtains

$$\begin{aligned} x(k+1) - x(k) \;&= \frac{\partial}{\partial k}x(k) = \underbrace{-\sum_{i=0}^{q-1}\omega_i\, a_i\sin(\omega_i k + \phi_i)}_{\text{in the continuum limit}} = \\ &= \sum_{i=0}^{q-1}\tilde{a}_i\sin(\omega_i k + \phi_i) \end{aligned} \qquad (11)$$

which again consists of orthogonal basis elements:

$(\sum_{k=0}^{q-1} \tilde{a}_i \sin(\omega_i k)\tilde{a}_j \sin(\omega_j k) = \delta_{ij})$.

Eq. (5) was obtained by the simulation and it is a constraint. Thus, any other additions of basis elements will only raise $\left|\frac{\partial}{\partial k}x(k)\right|_1$. Because if $\{\overrightarrow{x_i}\}$ is a set of orthogonal vectors and a vector is represented as $\vec{v} = \sum_{i=0}^{p} a_i \overrightarrow{x_i}$, an addition of another basis element will change the vector to $\vec{w} = \sum_{i=0}^{p+1} a_i \overrightarrow{x_i}$ $(a_{p+1} \neq 0)$ and the norms will be:

$$|\vec{v}| = \sum_{i=0}^{p}|a_i| < |\vec{w}| = \sum_{i=0}^{p+1}|a_i| = |\vec{v}| + |a_{p+1}|$$

(the inequality is also valid for the L_2 norm). Here the gradient's norm is increased from the same considerations.

Thus, a DCT diffuser provides a minimal gradient and the results of the TVAL3 are similar to reconstruction via the sum of the basis vectors. The DCT diffuser reconstruction complexity is $M \times p \times q$ whilst the complexity of TVAL3 is not deterministic and can greatly exceed this complexity as a single iteration requires more than $\left(M \times (m \times n - 1)\right)^2$ operations because of matrix multiplication.

In the following, the inventors simulated a realistic random mask/diffuser with a certain effective pattern size, i.e., autocorrelation length (ACL), and investigated how the ACL and the jumps over the diffuser / mask pattern influence the reconstruction of an object (region of interest). In particular, the inventors tested the effect of overlaps of pattern portions between different realizations of one mask pattern on the quality of reconstruction. The motivation for creating a quality reconstruction based on high-overlap realizations is the possibility of shortening the measurement time as well as reducing the physical size of the mask. Shortening of the measurement time may result from using smaller movements/jumps of the mask, while keeping the same number of realizations, whereas smaller movements may also contribute to reduction of the overall size of the mask.

The mask patterns designed for the simulations are random patterns based on a normal distribution, since this is a relatively easy format to produce in practice.

The simulations differ from each other in three parameters:

1. The compression factor, which determines the number of different realizations M, defined by:

$$M = \left\lfloor \frac{p \times q}{\text{compression factor}} \right\rfloor$$

2. The length of the mask auto-correlation. It should be kept in mind that the term "auto-correlation length" (ACL) as used here does not refer to auto-correlation in the mathematical - statistical meaning, but to the number of adjacent pixels (i.e., under assumed resolution of $p \times q$ pixels) whose value is the same. In other words, the ACL as used here expresses the degree to which the distribution of lateral sizes of the spaced-apart features **F** of the mask is self-similar laterally on the mask. The respective area of adjacent pixels whose value is the same is henceforward referred to as "effective pixel".

3. The size of the overlap between the realizations, which is determined by the size / value of the displacement (jump) on the mask pattern between any two realizations. Depending on the lateral axis, the jump may be referred to as $jump_x$ or $jump_y$, as in the example below.

Referring to **Fig. 4**, an exemplary mask pattern is shown and the pattern segments corresponding to four realizations based on the mask displacements ("$jump_x$") with respect to the X-axis. As shown in the figure, the pattern segments are designed so that their size is affected by combining two of the three parameters: $[p \times q + jump_x \times (M - 1)]$

Each pattern segment is simulated by:

(i) randomization of an $\left\lceil \frac{p}{ACL} \right\rceil \times \left\lceil \frac{q+jump_x \times (M-1)}{ACL} \right\rceil$ array from a normal distribution with mean = 0.5, variance = 0.3;

(ii) limiting the mask transfer (i.e., absorption) values to be between 0 to 1 in order to simulate absorption values and thus creating a difference between one realization and the other; and

(iii) duplicating each pixel to create a uniform area with a size of ACL×ACL - an "effective pixel".

This above-defined matrix D simulates a sandpaper-like mask pattern. Simulations of several types were performed: one-dimensional objects (region of interest); and two-dimensional objects when the overlap between different realizations is in the X-axis only.

In order to simplify the simulation, there is no reference to the progress of the field in the space between the pattern segment and the single-pixel detector, and it is assumed that this is the same field at both points, and the field can be linked to a system

where the detector is attached. In addition, in the first stage, no-noise simulations were performed, simulating a simple system in which the following two conditions are met:

1. A uniform beam without source noise - the radiation from the source has a constant intensity in space (as opposed to e.g., a Gaussian beam) and in addition the source is uniform without noise, both in time and in space.

2. A pattern segment with perfect effective pixels so that the value of each effective pixel is uniform.

In practice, the two conditions above are not met in the physical system, where the source noise impairs the quality of the reconstruction while the differences in transfer values within an effective pixel in the mask improve it.

To examine the effect of source noise on the quality of the reconstruction, several simulations were performed with the source noise added. In order to isolate the effect of the source noise which is expected to impair the quality of the restoration, no noise was introduced for this stage for the mask itself.

A number of quality parameters were calculated with the purpose of examining the quality of the reconstructions quantitatively: PSNR - peak signal-to-noise ratio, SSIM - structural similarity index measure, relative error, and mean squared error.

For a noise-free $p \times q$, monochrome image K and a noisy reconstruction U, the PSNR (in dB) is defined as

$$\mathrm{PSNR} = 10 \cdot \log_{10}\left(\frac{\mathrm{MAX}_K^2}{\mathrm{MSE}(U,K)}\right) \qquad (12)$$

The SSIM is:

$$\mathrm{SSIM}(U,K) = [l(U,K)]^{\alpha} \cdot [c(U,K)]^{\beta} \cdot [s(U,K)]^{\gamma} \qquad (13)$$

where:

$$l(U,K) = \frac{2\mu_U\mu_K + c_1}{\mu_U^2 + \mu_K^2 - c_1}, \quad c(U,K) = \frac{2\sigma_U\sigma_K + C_2}{\sigma_U^2 + \sigma_K^2 - C_2}, \quad s(U,K) = \frac{\sigma_{UK} + C_3}{\sigma_U + \sigma_K + C_3},$$

$\alpha = \beta = \gamma = 1, C_1 = 0.01L,\ C_2 = 0.03L, C_3 = \frac{C_2}{2}$, L =1 (the dynamic range of the pixel values), μ_i, σ_U^2 are the mean and the variance of U respectively, and the same for K.

For simplicity, movement in one direction (x direction) over the mask was assumed. The simulated mask pattern was chosen with an ACL of c pixels that moves with constant jumps of length j and undergoes M measurements of an object with a size of $p \times q$ pixels by drawing a $\left\lceil \frac{p}{c} \right\rceil \times \left\lceil \frac{q+j(M-1)}{c} \right\rceil$ normal random array (mean = 0.5,

variance = 0.3) and replacing each element of the array with an array of the size $c \times c$ with the original element repeated inside. This creates a virtual pixel matrix of the mask pattern.

To simulate a realistic mask pattern, the absorption property of the different features of the pattern to the X-ray radiation is between 0 and 1. The above distribution was chosen in order to simulate a random, e.g., a sandpaper-like mask pattern However, many other kinds of distributions could have been chosen with similar results achieved (it will be especially apparent when the mask pattern is represented in a matrix form below).

A $2D$ object can be rearranged in a $1D$ form and thereby the discussion of the $1D$ case will still be valid.

The first investigation concerns the case of jumps which are integer multiples of the ACL (c). In the $1D$ ($p = 1$) case a block matrix is obtained:

$$D = \begin{pmatrix} [a_{00} & \cdots & a_{00}] & \cdots & [a_{0q} & \cdots & a_{0q}] \\ & \vdots & & \ddots & & \vdots & \\ [a_{N0} & \cdots & a_{N0}] & \cdots & [a_{Nq} & \cdots & a_{Nq}] \end{pmatrix} \quad (14)$$

The constraints are:

$$D\vec{x} = \vec{b} \quad (15)$$

This can be rewritten as:

$$\widetilde{D}\vec{\chi} = \begin{pmatrix} a_{00} & \cdots & a_{0q} \\ \vdots & \ddots & \vdots \\ a_{N0} & \cdots & a_{Nq} \end{pmatrix} \vec{\chi} = \vec{\beta} \quad (16)$$

whilst $\vec{\beta} = \vec{b}/c$.

A solution for (16) is also a solution for (15) in a sense that every element in χ is repeated in x for c (i.e., ACL) times.

$$x_i = \chi_{\left\lfloor \frac{i}{c} \right\rfloor} \quad (17)$$

For computational ghost imaging (CGI), the Total Variation Algorithm 3 (TVAL3) is used, which tries to minimize (18):

$$\mathcal{L} = \alpha \sqrt{\sum_i \left(\sum_j D_{ij}\, x_j - b_i \right)^2} + \gamma \sum_j \left| x_{j+1} - x_j \right| \quad (18)$$

with $\alpha \gg \gamma$.

The solution in (17) fits perfectly to the reduction of the norm $|\nabla x|_1 = \sum_j |x_{j+1} - x_j|$ because it reduces the average gradient. The larger c is, the more explicitly one expects to observe this behavior because the larger is the value of c, the lower is the average gradient.

Let us consider the dimensions of matrix $\widetilde{D}$ (i.e., $M \times \left\lceil \frac{q}{c} \right\rceil$). The dimensions of D were $M \times q$, with $M < q$, because of the compression. Now, $\left\lceil \frac{q}{c} \right\rceil < q$ and one might even have $\left\lceil \frac{q}{c} \right\rceil < M$. So, these computations are valid under $M > \left\lceil \frac{q}{c} \right\rceil$. To reduce the gradient, $\widetilde{D}\vec{\chi} = \vec{\beta}$ is solved under $M > \left\lceil \frac{q}{c} \right\rceil$ employing TVAL3.

A convenient way to reorganize D is by periods, which means rearranging the rows so that each set of rows will have the same block structure as in (14). The higher the number of the sets, the less $|\nabla x|_1$ will cause a block structure as in (16) and the number of such sets is given by $\frac{\text{ACL}}{\text{gcd(ACL,Jump)}}$ (gcd = greatest common divider).

Table 1 below shows the fraction $\frac{\text{ACL}}{\text{gcd(ACL,Jump)}}$ for several choices of the ACL and jump. Larger integers in the **Table 1** correspond to a higher probability for a better reconstruction. These numbers indicate the trend expected in the simulation.

Table 1

ACL \ Jump	2	4	7	13	27	40	70	100
2	1	1	2	2	2	1	1	1
4	2	1	4	4	4	1	2	1
7	7	7	1	7	7	7	1	7
10	5	5	10	10	10	1	1	1
13	13	13	13	1	13	13	13	13
20	10	5	20	20	20	1	2	1

Table 2 below shows the PSNR of the simulation under compression ratio (CR) of 20 times. To prove the consistency of the results, each value was obtained as a mean of 100 simulations. It can be seen that for the larger ACL values, theory and simulation coincide to a large extent.

Table 2

ACL \ Jump	2	4	7	13	27	40	70	100
2	15.34	17.38	18.30	18.39	18.15	17.94	18.12	18.06
4	15.47	19.53	19.77	19.69	19.70	20.25	19.64	20.28
7	17.20	21.66	20.41	22.17	22.16	22.21	20.40	22.16
10	20.95	21.52	21.06	21.13	21.17	18.79	18.78	18.78
13	20.56	20.68	20.71	17.65	20.75	20.76	20.75	20.75
20	19.53	19.17	19.60	19.62	19.62	16.19	17.96	16.19

Figs. 5B to 5F show examples of (simulated) reconstructions of an original image shown in **Fig. 5A**. As already mentioned above, all the mask patterns were derived from a normal distribution with $\mu = 0.5$ and $\sigma = 0.3$.

The main simulation result demonstrates that an image of the region of interest can be better reconstructed with jumps that are smaller than the ACL (and consequently, the mask can be smaller). This can be seen, for example, comparing the PSNR values in rows corresponding to ACL=13 or ACL=20 in **Table 2** and comparing the image quality of **Fig. 5D** (ACL=7, jump = 13) and **Fig. 5E** (ACL=10, jump = 7). Though, for an ACL=7 for example, Jump= 13 is better than Jump= 4 but a bigger jump, e.g., Jump= 40 or Jump= 100 pixels (refer to PSNR values in **Table 2**) does not seem to improve much the reconstruction quality (i.e. increase PSNR).

It is to be noted that the results of the simulation show that the jump (i.e., displacement step of mask pattern) is to be of an optimal size with respect to the ACL. **Table 1** shows that when the jump is an exact multiple of ACL the reconstruction is of worse quality. This is confirmed by PSNR values in **Table 2**, belonging to matrix values corresponding to $\frac{\text{ACL}}{\text{gcd(ACL,Jump)}} = 1$ in **Table 1**, and by comparing the reconstruction results of **Fig. 5B** (ACL=13, jump = 13) with, e.g., reconstruction results of **Fig. 5E** (ACL=10, jump = 7). Too small jumps are not optimal as well, as can be seen in Tables 1 and 2. Thus, reconstruction examples in **Figs. 5B to 5F** demonstrate that increasing the jump does not necessarily lead to a better recovery, and in some cases, it even decreases the quality of recovery (compare, for example **Fig. 5E** (ACL=10, jump = 7) and **Fig. 5F** (ACL=20, jump = 27)).

In some embodiments, the optimization processes, such as the process for optimizing the mask structure, are done using ML tools, such as support vector-machine and deep neural networks.

As described above, the present invention utilizes designing of the mask pattern. In some examples, the mask pattern is designed with both sufficient randomness and spatial thickness variance. The optimal mask pattern design is selected, which provides the optimal results, i.e. best image quality with lowest required dose. As also described above, the sparsity nature of the objects (regions of interest) is considered, for example, for various organs in the human body, to determine the reduction of the dose and the number of realizations needed to enable high-quality image reconstruction. The latter may utilize the GI-based simulations combined with compressed sensing (e.g., including pseudo-inverse and sparsity constraint approaches) and/or ML tools. The structure of the mask pattern may be further optimized by obtaining the cost function, which is the number of required realizations for obtaining the object's image with the best SNR. In order to obtain the cost function, ML tools, such as Support Vector Machine and deep learning using Artificial Neural Networks, may be used.

Reference is made to **Fig. 6A** schematically illustrating, by way of a block diagram, the use of ML tools in designing the optimal mask structure (mask pattern parameters including those relating to the thickness variation of the mask structure). A set of training images is used to design a set of training mask patterns that serve as input for a GI-based simulation which includes simulation of the inspection (i.e., imaging) system and the subsequent GI-based algorithm of image reconstruction (i.e. compressed sensing correlation-based image processing). The so-reconstructed (by simulation) set of training images, together with the original training images serve as an input to build a deep neural network (DNN) model.

As noted above, the DNN model, optimizing the mask pattern, is obtained using a cost function which is the number of needed realizations for obtaining the object's image with the best SNR. The training stage produces a set of parameters, i.e., the weights matrix of the network (representing the optimal randomness and spatial thickness variance), which minimizes a loss function over the training data (i.e. providing minimum number of realizations with the best SNR). Once the weights matrix is produced, the network can be used to either predict class labels for a new set of observations, or to perform multi-variable regression. Once the DNN model is built, a group of testing

images is again subjected to simulation of the inspection (i.e., imaging) system and the subsequent GI-based algorithm of image analysis, using the optimal set of mask pattern parameters obtained during the training stage. The reconstructed testing images are input into the DNN model and the obtained predicted images are compared to the reconstructed ones via fitting (iterative procedure) to optimize the weights.

In the following, figures the results of simulations for resolution improvement are presented.

Fig. 7A shows a high-resolution chest X-ray image taken from images' bank to serve as an input for the simulation. In **Fig. 7B** the inventors downgraded the image of **Fig. 7A** to simulate lower resolution in existing imaging embodiments. Compared to the downgraded image (**Fig. 7B**), the techniques of GI according to the present invention, i.e., using each pixel as bucket detector to which GI is applied, provide better restoration of the image and achieve advantageous resolution (**Fig. 7C**).

Another example, demonstrating a simulation of compression for medical imaging is shown in **Figs. 8A** and **8B**. **Fig. 8A** shows an original X-ray image taken from images' bank, taken as a reference. The inventors performed a simulation of the above-described imaging technique, similar to the one described in relation to **Figs. 7A** to **7C**, however, this time using a compression ratio of 30 and utilizing a DCT (Discrete Cosine Transform) basis as described in detail above. The result of the simulation is shown in **Fig. 8B**. It can be appreciated that the high compression factor used did not compromise the image resolution and proves that compressed sensing correlation-based imaging and DCT basis according to the techniques of the present invention may provide high-resolution images while reducing the dose of X-ray radiation due to the mask design.

Reference is made to **Figs. 9A** and **9B** which illustrate the imaging of the Hebrew letter 'Aleph' (א) using an X-ray tube source. **Fig. 9A** shows the image obtained by direct imaging (with no spatial intensity coding), whereas **Fig. 9B** was obtained by the technique of the invention utilizing the above-described mask design. Tube X-ray sources are currently used for medical imaging where radiation dose is critically controlled, as opposed to high-brightness synchrotron sources used in research applications. The image of **Fig. 9B** contains 5,000 pixels, while the inventors used only 500 realizations for reconstruction (the measurement time of one realization was about 1 sec). The object was the Hebrew letter Alef, which was made of a 30 nm gold on a Quartz membrane. The

transmission of the gold is 98.8% at 8 keV (the image was obtained by using a lab (tube X-ray) source, which is a copper-based anode that radiates at 8.04 keV).

CLAIMS:

1. A masking assembly for use in inspecting a region of interest by creating structured high photon energy radiation to interact with the region of interest, said masking assembly comprising: at least one mask structure, the mask structure having a predetermined effective thickness t, and comprising a mask pattern formed by an arrangement of spaced-apart features of absorption properties with respect to said high photon energy radiation different from spaces between said features, said arrangement of said features along a lateral dimension of the pattern defining a predetermined effective pattern size P, wherein the features have a characteristic lateral size l providing a substantially high aspect ratio t/l.

2. The mask assembly according to claim 1, wherein the mask structure has a spatial modulation of thickness along the pattern within said effective thickness t.

3. The mask assembly according to claim 1 or 2, wherein said mask structure is a disk, said spaced-apart features of the mask pattern being arranged along a substantially circular path.

4. The mask assembly according to any one of the preceding claims, comprising a drive mechanism configured and controllably operable to implement successive lateral movements of said mask pattern with a predetermined lateral jump j to thereby enable successive inspection realizations through different segments of the mask pattern, respectively, wherein a value of said lateral jump $j \neq N \times P$, N being an integer.

5. The mask assembly according to claim 4, wherein said predetermined lateral jump j is smaller than P.

6. The mask according to any one of the preceding claims, wherein said aspect ratio t/l is at least 10.

7. The mask assembly according to any one of the preceding claims, wherein the mask pattern is formed by relatively highly absorbing features arranged in the spaced-apart relationship in a relatively low-absorbing substrate with respect to said high photon energy radiation.

8. The mask assembly according to any one of claims 1 to 6, wherein the mask pattern is formed by relatively low-absorbing features arranged in the spaced-apart relationship in a relatively highly absorbing substrate with respect to said high photon energy radiation.

9. The mask assembly according to claim 7 or 8, wherein relatively high absorbing material of the mask pattern comprises metal material composition.

10. The mask assembly according to claim 9, wherein said metal material composition comprises at least one of the following: tungsten, platinum, silver, gold and tantalum.

11. The mask assembly according to claim 7, wherein said mask pattern is produced by metal printing of said spaced-apart features, followed by laser milling.

12. The mask assembly according to claim 11, wherein metal material being printed comprises at least one of the following: tungsten, platinum, silver, gold and tantalum.

13. The mask assembly according to any one of claims 8 to 10, wherein said mask pattern is in the form of distribution of pores in the relatively highly absorbing substrate.

14. The mask assembly according to claim 13, wherein said substrate is made from one of the following: Limestone, Mortar, AlCu, MgZn.

15. The mask assembly according to any one of the preceding claims, wherein the mask pattern comprises an arrangement of said features providing desired sparsity in a predetermined base selected in accordance with base of sparsity in the region of interest being inspected.

16. The mask assembly according to any one of claims 1 to 14, wherein the mask pattern comprises a random arrangement of said spaced-apart features.

17. The mask assembly according to any one of claims 1 to 14, wherein the arrangement of said spaced-apart features of the mask pattern is selected in accordance with a function corresponding to discrete cosine transform.

18. An inspection system for inspecting a region of interest, the inspection system comprising: a measurement device configured and operable to perform a plurality of successive measurements of the region of interest by implementing a corresponding plurality of interactions of the region of interest with high photon energy radiation beams having predetermined different spatially encoded intensity profiles, and a detection system comprising at least one radiation detector device successively collecting radiation responses of the region of interest to said interactions and generating measured data indicative thereof, wherein said high photon energy radiation beams having predetermined different spatially encoded intensity profiles are sequentially produced by passing an initial high photon energy radiation beam through the masking assembly of any one of claims 1 to 17.

19. The inspection system according to claim 18, wherein said at least one radiation detector device is configured and operable to collect said response of the region of interest comprising Compton scattering of the region of interest.

20. The inspection system according to claim 19, wherein said at least one radiation detector device is accommodated for collecting at least one of back propagating and forward propagating radiation of said Compton scattering of the region of interest.

21. The inspection system according to any one of claims 18 to 20, comprising a control system configured and operable to process said measured data, thereby enabling reconstruction of image of the region of interest from said measured data by applying thereto at least one of compressed sensing based correlation processing and/or machine learning based processing, and generate data indicative of reconstructed image of the region of interest.

22. An inspection system for inspecting a region of interest, the inspection system comprising:

a measurement device configured and operable to perform a plurality of successive measurements of the region of interest by implementing a corresponding plurality of interactions of the region of interest with high photon energy radiation beams of X- or gamma-radiation having predetermined different spatially encoded intensity profiles, and a detection system comprising at least one radiation detector device configured and operable to successively collect radiation responses of the region of interest to said interactions and generate measured data indicative thereof, wherein said at least one radiation detector device is configured and operable to collect said response of the region of interest comprising Compton scattering of the region of interest including at least one of back propagating and forward propagating radiation of said Compton scattering of the region of interest, thereby enabling reconstruction of image of the region of interest from said measured data by applying thereto at least one of compressed sensing based correlation processing and machine learning based processing.

23. The inspection system according to claim 22, comprising a communication utility for communicating said measured data to a control system configured to perform said at least one of the compressed sensing based correlation processing and the machine learning based processing of the measure data and generate the reconstructed image of the region of interest.

24. The inspection system according to claim 22, comprising a control system configured to perform said at least one of the compressed sensing based correlation processing and the machine learning based processing.

25. The inspection system according to any one of claims 22 to 24, wherein the measurement device comprises:

a) a source of the X-ray or gamma-ray radiation configured to provide an input beam of said radiation;

b) a mask assembly accommodated in a general propagation path of said input beam, the mask assembly comprising at least one mask structure being configured and controllably operated to sequentially induce different intensity fluctuations on the input beam, thereby sequentially producing beams of the X- or gamma-radiation having predetermined different spatially encoded intensity profiles, the mask structure having a predetermined effective thickness t, and comprising a mask pattern formed by an arrangement of spaced-apart features of absorption properties with respect to said high photon energy radiation different from spaces between them, said arrangement of said features along a lateral dimension of the mask pattern defining a predetermined effective pattern size P, wherein the features have a characteristic lateral size l providing a substantially high aspect ratio t/l.

26. The inspection system according to claim 25, wherein said mask structure has a spatial modulation of thickness along the mask pattern within said effective thickness t.

27. The inspection system according to claim 25 or 26, wherein said mask structure is a disk, said spaced-apart features of the mask pattern being arranged along a substantially circular path.

28. The inspection system according to any one of claims 25 to 27, comprising a drive mechanism configured and controllably operable to implement successive lateral displacements between the general propagation path of the input beam and said mask pattern with a predetermined lateral jump j to thereby enable successive inspection realizations through different segments of the mask pattern, respectively, wherein a value of said lateral jump $j \neq N \times P$, N being an integer.

29. The inspection system according to claim 28, wherein said predetermined lateral jump j is smaller than P.

30. The inspection system according to any one of claims 25 to 29, wherein said aspect ratio t/l is at least 10.

31. The inspection system according to any one of claims 25 to 30, wherein the mask pattern is formed by relatively highly absorbing features arranged in the spaced-apart relationship in a relatively low-absorbing substrate with respect to said high photon energy radiation.

32. The inspection system according to any one of claims 25 to 30, wherein the mask pattern is formed by relatively low-absorbing features arranged in the spaced-apart relationship in a relatively highly absorbing substrate with respect to said high photon energy radiation.

33. The inspection system according to claim 31 or 32, wherein relatively high absorbing material of the mask pattern comprises metal material composition.

34. The inspection system according to claim 33, wherein said metal material composition comprises at least one of the following: Tungsten, Platinum, Silver, Gold and Tantalum.

35. The inspection system according to any one of claims 25 to 34, wherein the mask comprises at least one of 3D printed structure, and porous materials.

36. The inspection system according to claim 31, wherein said mask pattern is produced by metal printing of said spaced-apart features, followed by laser milling.

37. The inspection system according to claim 36, wherein metal material being printed comprises at least one of the following: tungsten, platinum, silver, gold and tantalum.

38. The inspection system according to any one of claims 32 to 34, wherein said mask pattern is in the form of distribution of pores in the relatively highly absorbing substrate.

39. The inspection system according to claim 38, wherein said substrate is made from one of the following: Limestone, Mortar, AlCu, MgZn.

40. The inspection system according to any one of claims 25 to 39, wherein the mask pattern comprises an arrangement of said features providing desired sparsity in a predetermined base selected in accordance with base of sparsity in the region of interest being inspected.

41. The inspection system according to any one of claims 25 to 39, wherein the mask pattern comprises a random arrangement of said spaced-apart features.

42. The inspection system according to claim 40, wherein the arrangement of the spaced-apart features of the mask pattern is selected in accordance with a function corresponding to discrete cosine transform.

43. A method for inspecting a region of interest by X-rays or gamma rays radiation comprising:

i) producing an input beam of X-ray or gamma-ray radiation directed along a general propagation path towards the region of interest;

ii) scanning, by the input beam on its way towards the region of inters, a mask pattern, thereby sequentially inducing different intensity fluctuations in the input beam and producing a sequence of beams of the X- or gamma-radiation having predetermined different spatially encoded intensity profiles propagating towards the region of interest to successively interact with the region of interest and induce radiation a corresponding sequence of radiation responses of the region of interest comprising Compton scattering of the region of interest, said scanning being implemented by successive lateral displacements between the general propagation path of the input beam and said mask pattern with a predetermined lateral jump j of a value satisfying a condition $j \neq NxP$, where N is an integer and P is a predetermined effective pattern size P of the mask pattern;

iii) detecting said sequence of the radiation responses comprising at least one of back propagating and forward propagating radiation of said Compton scattering of the region of interest and generating measured data indicative thereof, thereby enabling reconstruction of image of the region of interest from said measured data by applying thereto at least one of the compressed sensing based correlation processing and the machine learning based processing.

44. The method according to claim 43, wherein said mask structure has a predetermined effective thickness t, and comprises the mask pattern formed by an arrangement of spaced-apart features of different absorption properties with respect to said X-ray or gamma-ray radiation as compared with spaces between them, said arrangement of said features along a lateral dimension of the pattern defining said predetermined effective pattern size P, wherein the features have a characteristic lateral size l providing a substantially high aspect ratio t/l.

45. The method according to claim 43 or 44, wherein said mask structure has a spatial modulation of thickness along the pattern within said effective thickness t.

46. The method according to any one of claims 43 to 45, wherein the mask pattern comprises an arrangement of features providing desired sparsity in a predetermined base selected in accordance with base of sparsity in the region of interest being inspected.

47. The method according to any one of claims 43 to 45, wherein the mask pattern comprises a random arrangement of spaced-apart features.

48. The method according to claim 46, wherein the mask pattern comprises features arranged in accordance with function corresponding to discrete cosine transform.

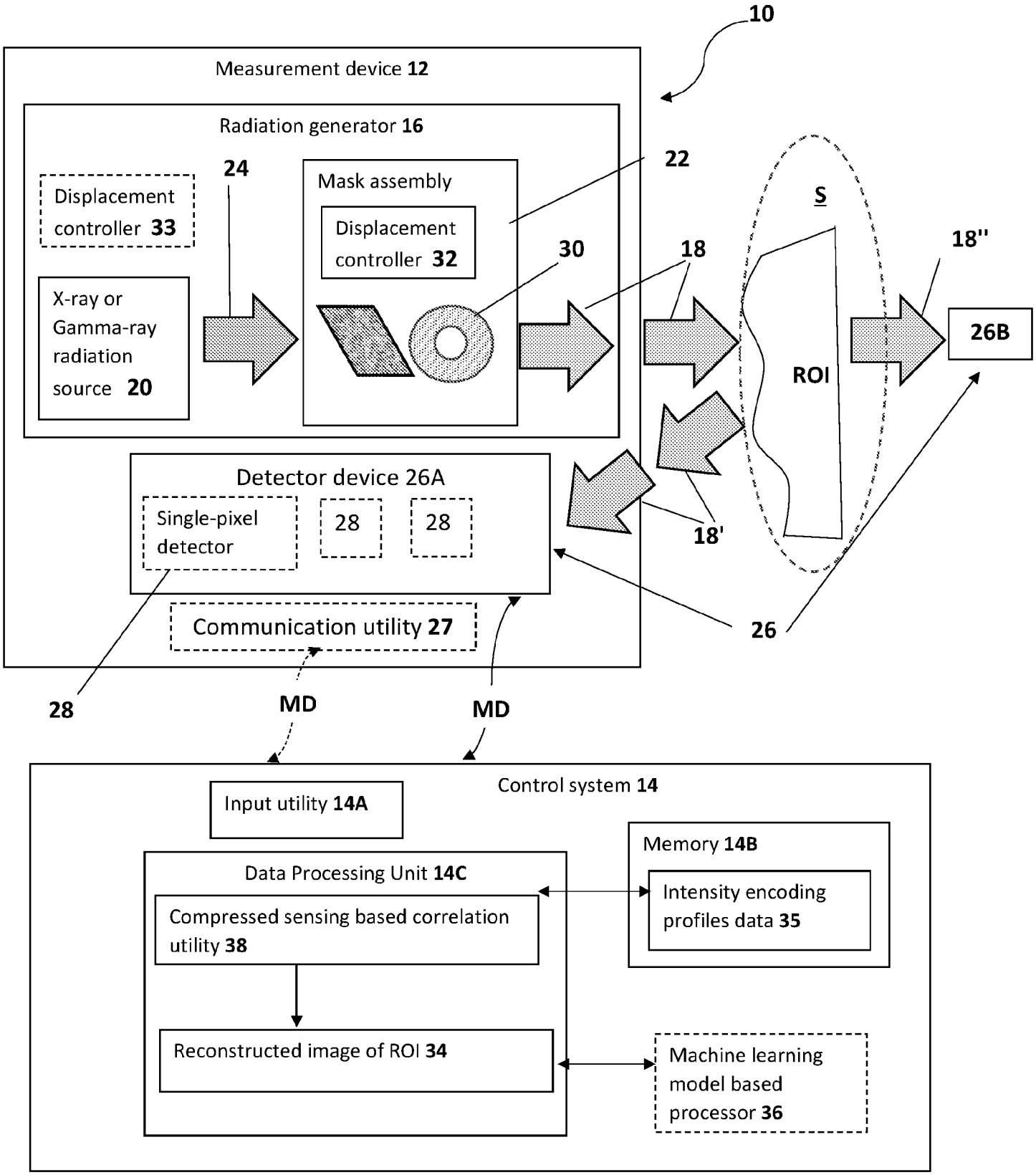

10
Measurement device 12
Radiation generator 16
Displacement controller 33
24
X-ray or Gamma-ray radiation source 20
Mask assembly
Displacement controller 32
22
30
18
S
ROI
18''
26B
Detector device 26A
Single-pixel detector
28
28
18'
Communication utility 27
26
28
MD
MD
Control system 14
Input utility 14A
Memory 14B
Data Processing Unit 14C
Intensity encoding profiles data 35
Compressed sensing based correlation utility 38
Reconstructed image of ROI 34
Machine learning model based processor 36

Fig. 1

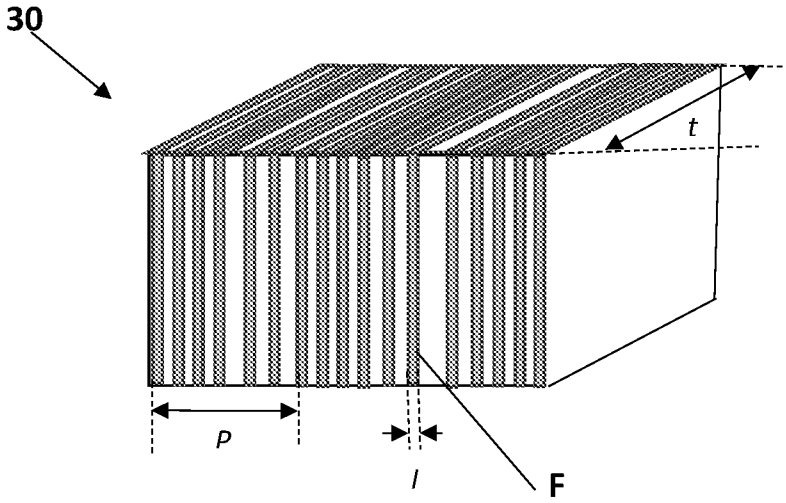

30
t
P
l
F

Fig. 2

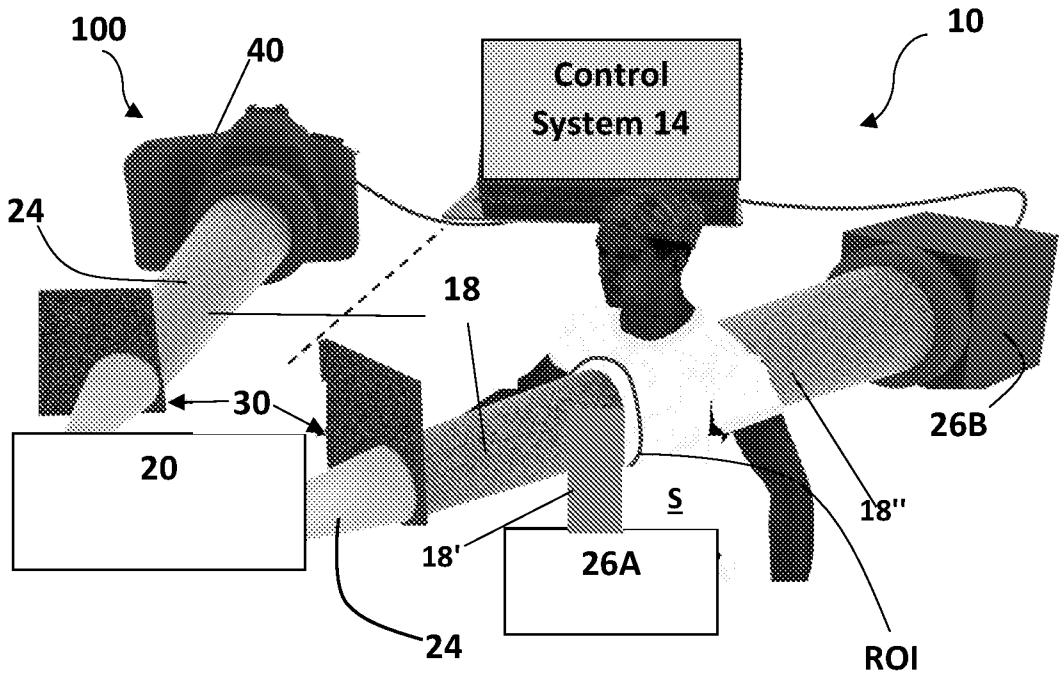

100
40
Control System 14
10
24
18
30
20
26B
S
18''
18'
26A
24
ROI

Fig. 3A

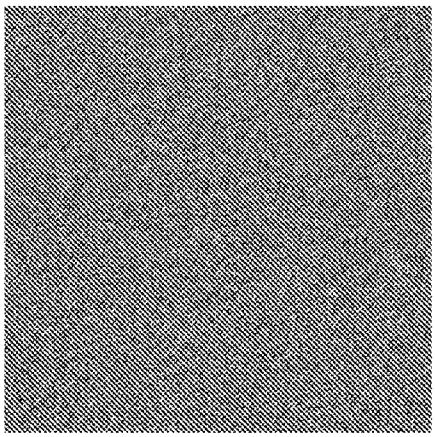


Fig. 3B

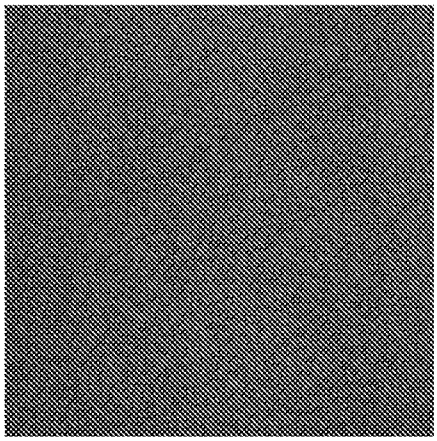


Fig. 3C

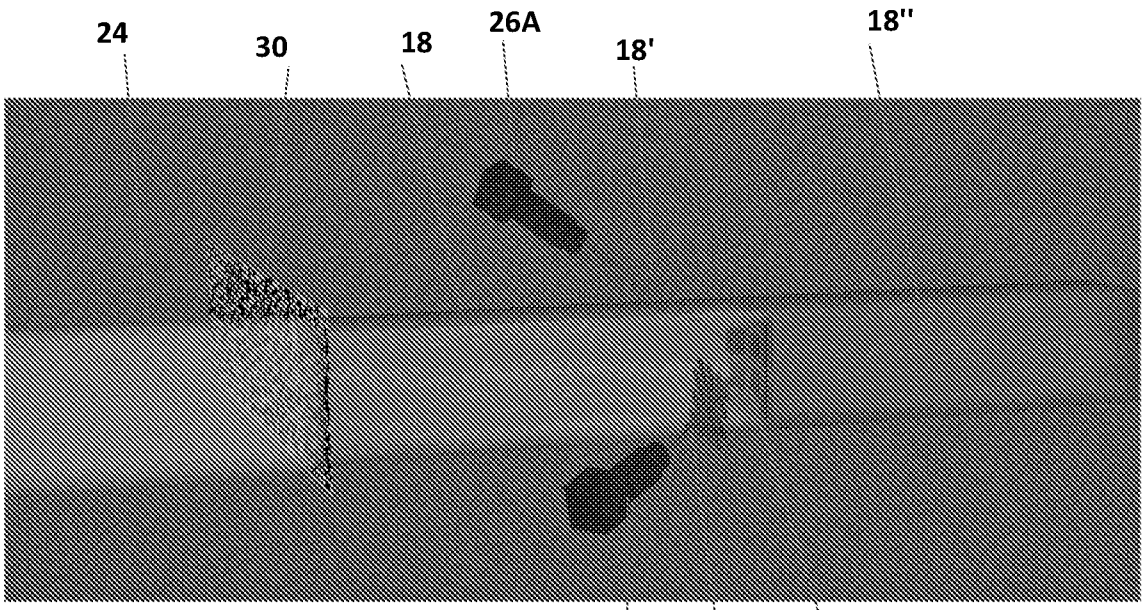


Fig. 3D

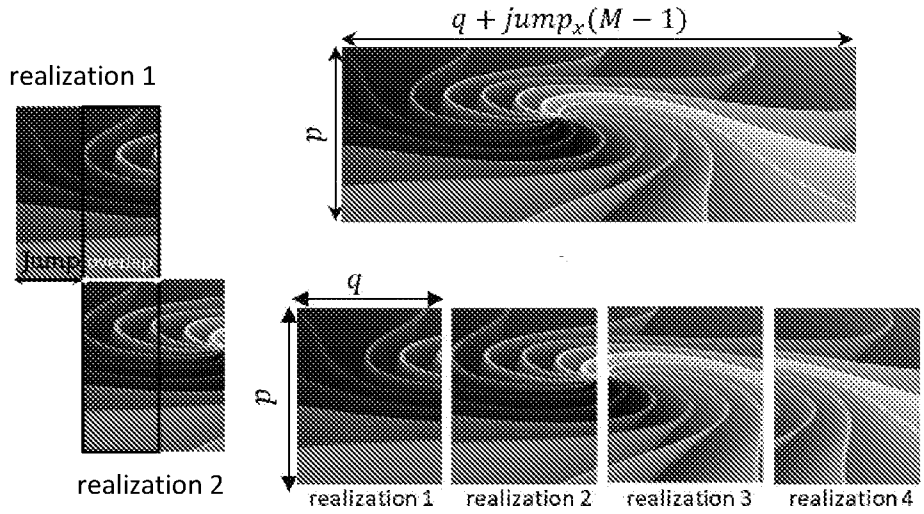

realization 1
realization 2
jump
$q + jump_x(M-1)$
p
q
p
realization 1
realization 2
realization 3
realization 4

Fig. 4

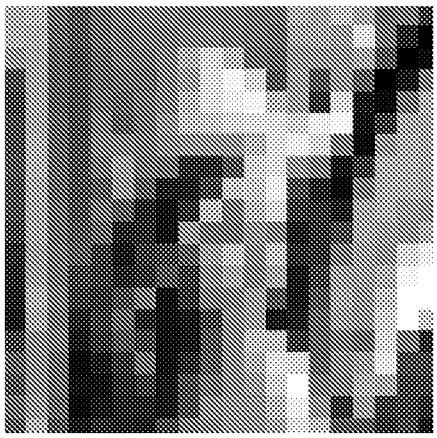
compression factor = 20

Fig. 5A



Original image

Fig. 5B



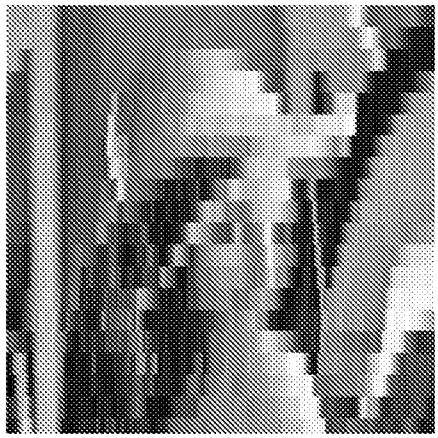
ACL =13, jump = 13

Fig. 5C



ACL =7, jump = 100

Fig. 5D



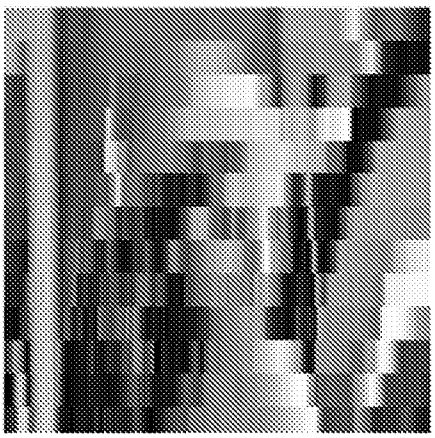
ACL =7, jump = 13

Fig. 5E



ACL =10, jump = 7

Fig. 5F



ACL =20, jump = 27

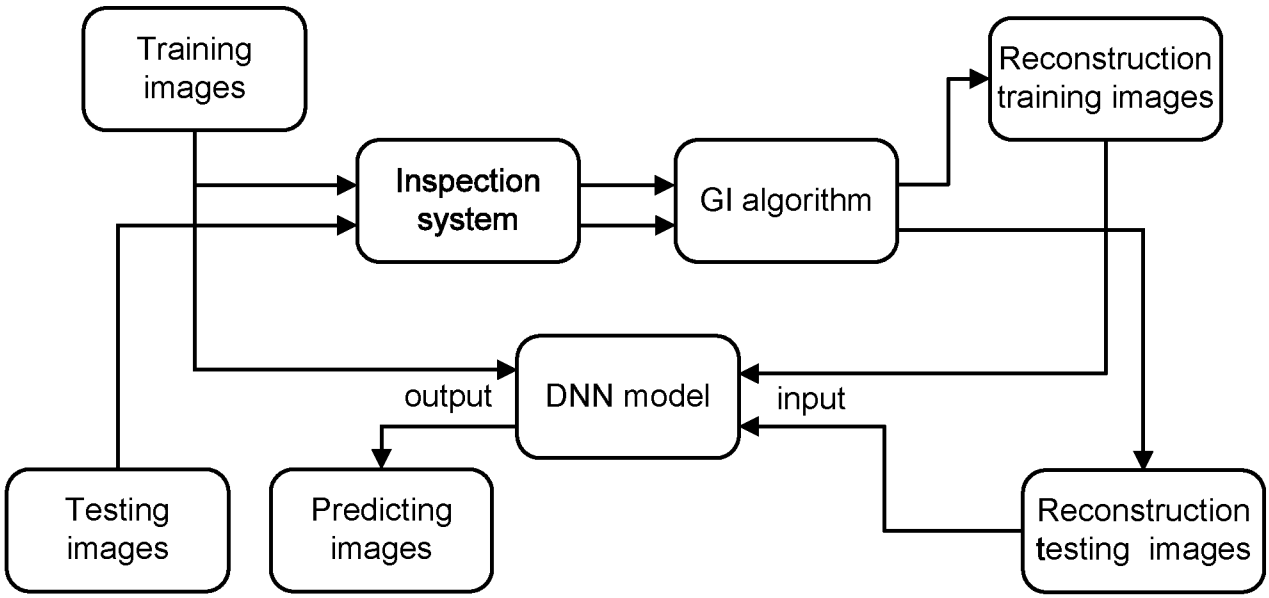

Training images
Inspection system
GI algorithm
Reconstruction training images
output
DNN model
input
Testing images
Predicting images
Reconstruction testing images

Fig. 6

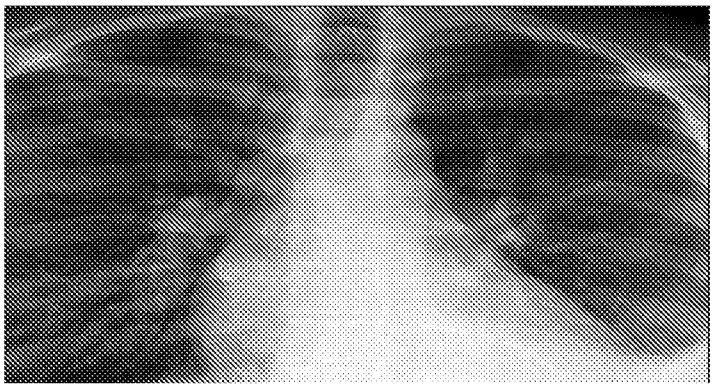


Fig. 7A

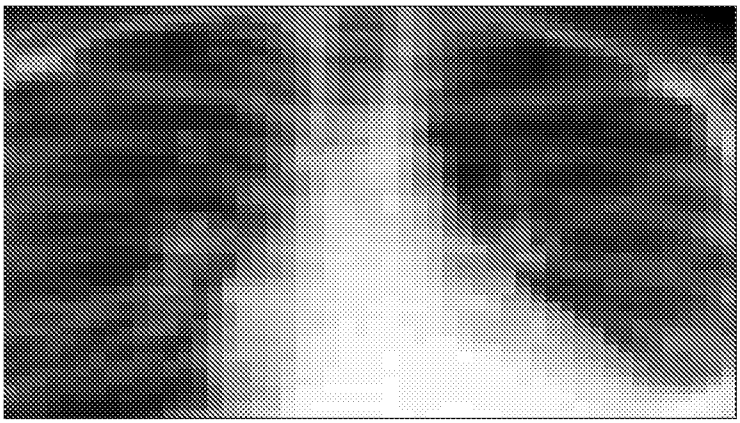


Fig. 7B

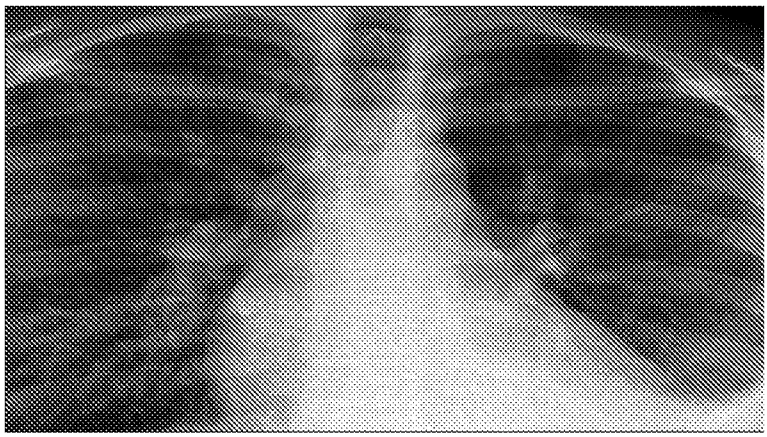


Fig. 7C

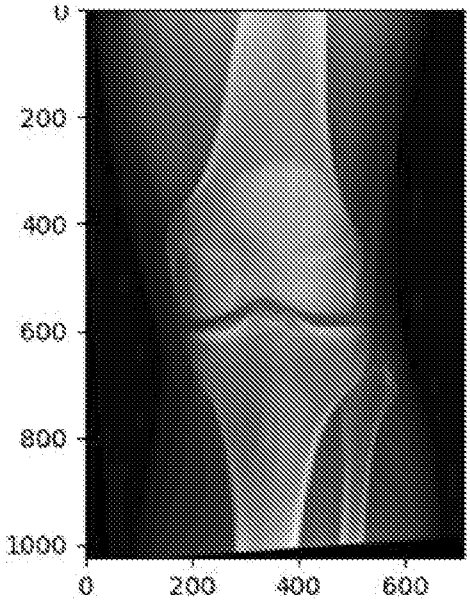

0
200
400
600
800
1000
0
200
400
600

Fig. 8A

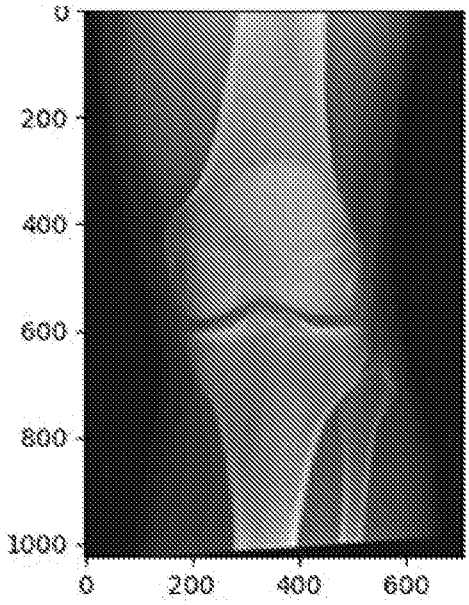

0
200
400
600
800
1000
0
200
400
600

Fig. 8B

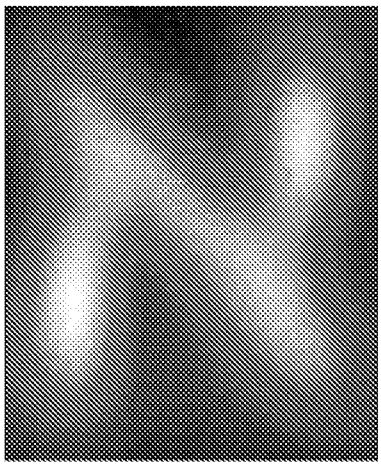


Fig. 9A

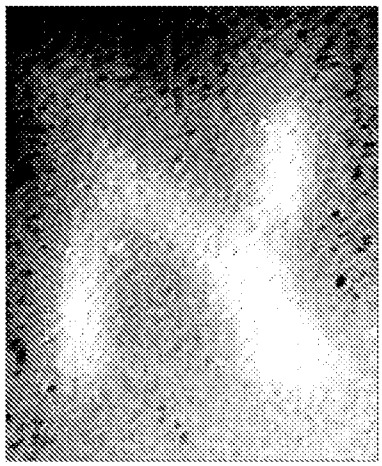


Fig. 9B

INTERNATIONAL SEARCH REPORT

International application No.
PCT/IL2022/050814

A. CLASSIFICATION OF SUBJECT MATTER

G01N 23/02(2022.01)i; ***G01N 23/203***(2022.01)i; ***G01T 1/29***(2022.01)i
CPC:G01N 23/02; G01N 23/203; G01T 1/295

According to International Patent Classification (IPC) or to both national classification and IPC

B. FIELDS SEARCHED

Minimum documentation searched (classification system followed by classification symbols)

G01N 23/02; G01N 23/203; G01T 1/29
CPC:G01N 23/02; G01N 23/203; G01T 1/295

Documentation searched other than minimum documentation to the extent that such documents are included in the fields searched

Electronic data base consulted during the international search (name of data base and, where practicable, search terms used)

Databases consulted: Orbit, Similari (AI-based) Search terms used: PHOTON+, mask+, pattern+, structur+, inspect+, interest+, region+, X- OR GAMMA+, RADIAT+

C. DOCUMENTS CONSIDERED TO BE RELEVANT

Category*	Citation of document, with indication, where appropriate, of the relevant passages	Relevant to claim No.
X	US 2008095298 A1 (Thermo Scientific Portable Analytical Instruments Inc.) 24 April 2008 (2008-04-24) The whole document	1-48
A	US 5606165 A (AIL Systems Inc.) 25 February 1997 (1997-02-25) The whole document	1-48
A	US 2020408940 A1 (Australian Nuclear Science and Technology Organization) 31 December 2020 (2020-12-31) The whole document	1-48
A	US 2002075990 A1 (Massachusetts Institute of Technology) 20 June 2002 (2002-06-20) The whole document	1-48

☐ Further documents are listed in the continuation of Box C. ☑ See patent family annex.

* Special categories of cited documents:
"A" document defining the general state of the art which is not considered to be of particular relevance
"D" document cited by the applicant in the international application
"E" earlier application or patent but published on or after the international filing date
"L" document which may throw doubts on priority claim(s) or which is cited to establish the publication date of another citation or other special reason (as specified)
"O" document referring to an oral disclosure, use, exhibition or other means
"P" document published prior to the international filing date but later than the priority date claimed
"T" later document published after the international filing date or priority date and not in conflict with the application but cited to understand the principle or theory underlying the invention
"X" document of particular relevance; the claimed invention cannot be considered novel or cannot be considered to involve an inventive step when the document is taken alone
"Y" document of particular relevance; the claimed invention cannot be considered to involve an inventive step when the document is combined with one or more other such documents, such combination being obvious to a person skilled in the art
"&" document member of the same patent family

Date of the actual completion of the international search	Date of mailing of the international search report
06 November 2022	**09 November 2022**

Name and mailing address of the ISA/IL	Authorized officer
Israel Patent Office **Technology Park, Bldg.5, Malcha, Jerusalem, 9695101,** **Israel** **Israel** Telephone No. **972-73-3927192** Email: **pctoffice@justice.gov.il**	**CHANIEL Gilad** Telephone No.

INTERNATIONAL SEARCH REPORT
Information on patent family members

International application No.
PCT/IL2022/050814

Patent document cited in search report	Publication date (day/month/year)	Patent family member(s)	Publication date (day/month/year)
US 2008095298 A1	24 April 2008	US 2008095298 A1	24 April 2008
		US 7623614 B2	24 November 2009
		AU 2007351440 A1	23 October 2008
		AU 2007351440 B2	06 December 2012
		CA 2665872 A1	23 October 2008
		CA 2665872 C	02 April 2013
		CN 101568855 A	28 October 2009
		EP 2076793 A2	08 July 2009
		EP 2076793 B1	06 January 2016
		JP 2010507811 A	11 March 2010
		WO 2008127385 A2	23 October 2008
		WO 2008127385 A3	16 July 2009
US 5606165 A	25 February 1997	US 5606165 A	25 February 1997
		AT 243327 T	15 July 2003
		AU 1256595 A	06 June 1995
		AU 1827697 A	11 August 1997
		CA 2242992 A1	24 July 1997
		CA 2242992 C	15 April 2008
		DE 69722938 D1	24 July 2003
		DE 69722938 T2	19 May 2004
		EA 199800639 A1	24 December 1998
		EA 000675 B1	28 February 2000
		EP 0920643 A1	09 June 1999
		EP 0920643 A4	09 June 1999
		EP 0920643 B1	18 June 2003
		ES 2205174 T3	01 May 2004
		IL 111436 D0	29 December 1994
		IL 111436 A	15 July 1998
		IL 125360 D0	12 March 1999
		IL 125360 A	14 June 2001
		IN 191992 B	07 February 2004
		JP 2000503393 A	21 March 2000
		JP 3919222 B2	23 May 2007
		JP 2006227024 A	31 August 2006
		KR 19990077306 A	25 October 1999
		KR 100388577 B1	19 August 2003
		TW 259848 B	11 October 1995
		TW 340909 B	21 September 1998
		WO 9514245 A1	26 May 1995
		WO 9726557 A1	24 July 1997
		ZA 97325 B	09 March 1998
		ZA 949105 B	21 July 1995
US 2020408940 A1	31 December 2020	US 2020408940 A1	31 December 2020
		US 11346964 B2	31 May 2022
		AU 2015263838 A1	22 December 2016
		AU 2015263838 A2	20 July 2017
		AU 2015263838 B2	26 September 2019
		CA 2949558 A1	26 November 2015
		CN 106663489 A	10 May 2017
		CN 106663489 B	27 March 2020

INTERNATIONAL SEARCH REPORT
Information on patent family members

International application No.
PCT/IL2022/050814

Patent document cited in search report	Publication date (day/month/year)	Patent family member(s)			Publication date (day/month/year)
		DK	3146527	T3	22 November 2021
		EP	3146527	A1	29 March 2017
		EP	3146527	A4	02 May 2018
		EP	3146527	B1	18 August 2021
		EP	3944260	A1	26 January 2022
		ES	2897650	T3	02 March 2022
		HU	E057042	T2	28 April 2022
		JP	2017522543	A	10 August 2017
		JP	6654578	B2	26 February 2020
		JP	2020060591	A	16 April 2020
		JP	6974424	B2	01 December 2021
		KR	20170018836	A	20 February 2017
		KR	102393273	B1	29 April 2022
		LT	3146527	T	25 February 2022
		MX	2016015292	A	20 June 2017
		MX	363049	B	06 March 2019
		PL	3146527	T3	07 February 2022
		RU	2016150551	A	25 June 2018
		RU	2016150551	A3	25 June 2018
		RU	2706736	C2	20 November 2019
		SG	10201808726R	A	29 November 2018
		SG	11201609671U	A	29 December 2016
		UA	123038	C2	10 February 2021
		US	2017322327	A1	09 November 2017
		US	10795036	B2	06 October 2020
		US	2022308244	A1	29 September 2022
		WO	2015176115	A1	26 November 2015
US 2002075990 A1	20 June 2002	US	2002075990	A1	20 June 2002
		US	6737652	B2	18 May 2004
		WO	02056055	A2	18 July 2002
		WO	02056055	A3	26 February 2004